nature immunology

Article

https://doi.org/10.1038/s41590-023-01637-4

Fungal microbiota sustains lasting immune activation of neutrophils and their progenitors in severe COVID-19

Received: 15 June 2023

Accepted: 6 September 2023

Published online: 23 October 2023

Check for updates

Takato Kusakabe[1,2], Woan-Yu Lin[1,2,3], Jin-Gyu Cheong[3,4], Gagandeep Singh[5,6], Arjun Ravishankar[4], Stephen T. Yeung[1,7], Marissa Mesko[1,2], Meghan Bialt DeCelie[1,2], Guilhermina Carriche[1,2], Zhen Zhao[4], Sophie Rand[4], Itai Doron[1,2], Gregory G. Putzel[2], Stefan Worgall[3,8], Melissa Cushing[4], Lars Westblade[4], Giorgio Inghirami[4], Christopher N. Parkhurst[1], Chun-Jun Guo[1,2,3,9], Michael Schotsaert[5,6], Adolfo García-Sastre[5,6,10,11,12], Steven Z. Josefowicz[3,4], Mirella Salvatore[1,13] & Iliyan D. Iliev[1,2,3,9]

Gastrointestinal fungal dysbiosis is a hallmark of several diseases marked by systemic immune activation. Whether persistent pathobiont colonization during immune alterations and impaired gut barrier function has a durable impact on host immunity is unknown. We found that elevated levels of *Candida albicans* immunoglobulin G (IgG) antibodies marked patients with severe COVID-19 (sCOVID-19) who had intestinal *Candida* overgrowth, mycobiota dysbiosis and systemic neutrophilia. Analysis of hematopoietic stem cell progenitors in sCOVID-19 revealed transcriptional changes in antifungal immunity pathways and reprogramming of granulocyte myeloid progenitors (GMPs) for up to a year. Mice colonized with *C. albicans* patient isolates experienced increased lung neutrophilia and pulmonary NETosis during severe acute respiratory syndrome coronavirus-2 infection, which were partially resolved with antifungal treatment or by interleukin-6 receptor blockade. sCOVID-19 patients treated with tocilizumab experienced sustained reductions in *C. albicans* IgG antibodies titers and GMP transcriptional changes. These findings suggest that gut fungal pathobionts may contribute to immune activation during inflammatory diseases, offering potential mycobiota-immune therapeutic strategies for sCOVID-19 with prolonged symptoms.

Severe acute respiratory syndrome coronavirus-2 (SARS-CoV-2), the causative agent of COVID-19, has infected more than 700 million people worldwide, causing over 7 million deaths to date[1]. In addition to all described symptoms[2], millions of individuals who have recovered from acute COVID-19 infection suffer postacute sequelae of COVID-19 (PASC) or long-COVID, manifesting with memory loss, fatigue and gastrointestinal (GI) distress[3]. Although mechanisms leading to disease exacerbation are still under investigation, immune dysregulation is a key characteristic of COVID-19 pathophysiology[4].

Studies have reported substantial involvement of the GI tract in the pathophysiology of several inflammatory diseases, including severe COVID-19 (sCOVID-19)[5–7]. Patients with COVID-19 present with altered gut microbial composition and gut barrier dysfunction, which could increase the translocation of bacterial products and toxins into

A full list of affiliations appears at the end of the paper. e-mail: iliev@med.cornell.edu

https://doi.org/10.1038/s41590-023-01637-4

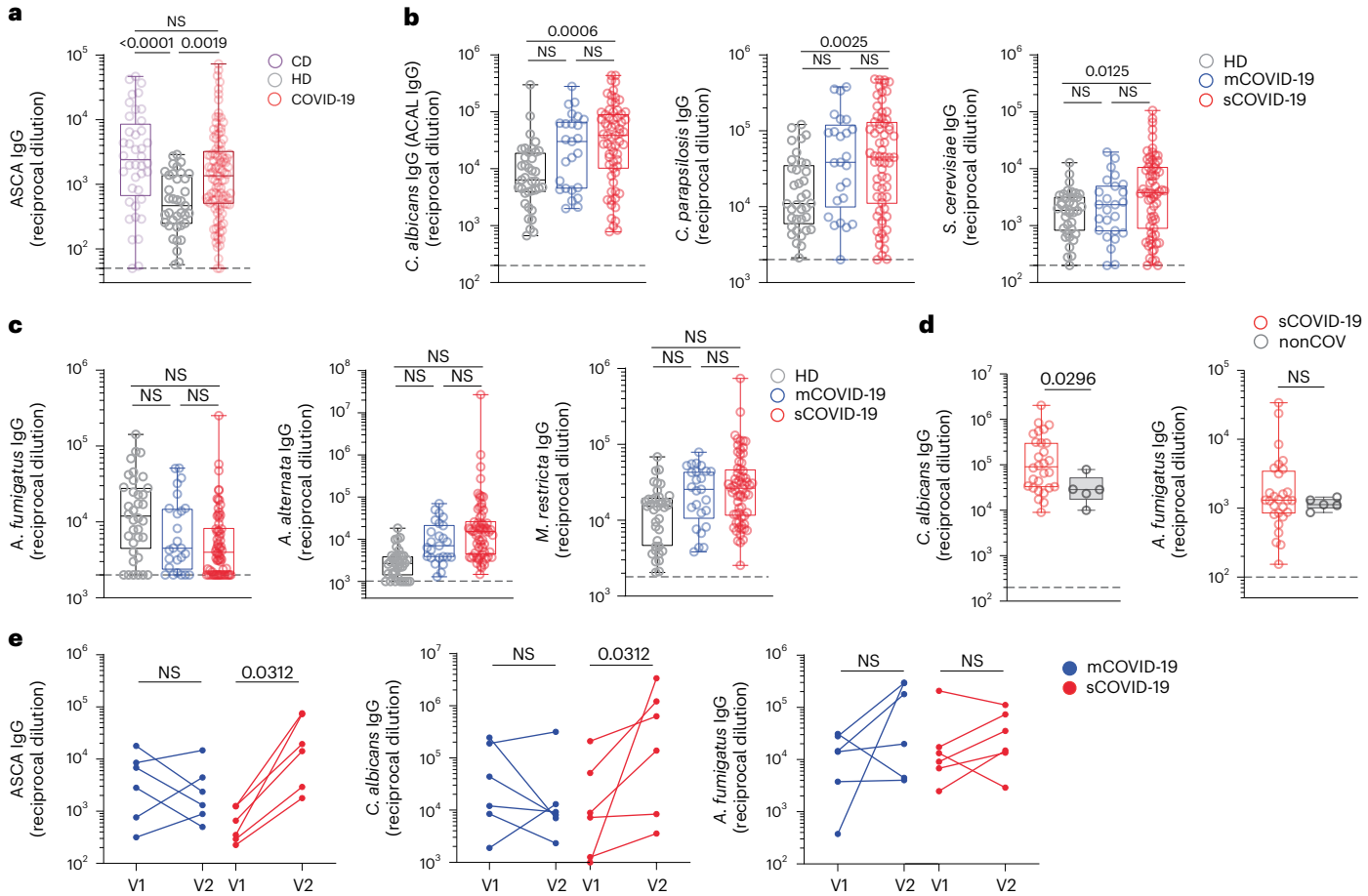

Fig. 1 | Antibodies to common intestinal fungi are elevated in patients with COVID-19. a, Plasma antibody titers of circulating IgG to fungal mannan (*Saccharomyces cerevisiae*; ASCA) in patients with CD ($n = 40$), healthy individuals (HD, $n = 36$) and patients with COVID-19 ($n = 91$). **b**,**c**, Plasma IgG antibody titers to *C. albicans* IgG (ACAL IgG), *C. parapsilosis* IgG and *S. cerevisiae* IgG (**b**) or *A. fumigatus* IgG, *A. alternata* IgG and *M. restricta* IgG (**c**) in HD ($n = 36$), mCOVID-19 ($n = 25$) and sCOVID-19 ($n = 66$; Extended Data Table 1). Mild and moderate patients were grouped together as mCOVID-19 for analysis against sCOVID-19 or HD. **d**, Plasma IgG antibody titers to *C. albicans* and *A. fumigatus* IgG in patients with sCOVID-19 ($n = 28$) and non-COVID-19 admitted in the intensive care unit (non-COV, $n = 5$; Extended Data Table 2). **e**, Longitudinal assessment of plasma IgG antibody titers to ASCA, *C. albicans* (ACAL) and *A. fumigatus* IgG in mCOVID-19 ($n = 6$) and sCOVID-19 ($n = 6$). Samples are collected at clinical diagnosis of infection or first administration (V1) and during the development of acute disease stage (V2; more than 2 weeks post-V1). All data are shown as endpoint titers normalized to ELISA reciprocal dilution. The dotted line indicates the limit of detection. For all boxplots, the center is drawn through the median of the measurement, and the lower and upper bounds of the box correspond to the first and third quartiles. The whiskers go down to the smallest value and up to the largest. Statistical significance was determined by the one-way ANOVA followed by Tukey's multiple comparison in **a**–**c**, a two-tailed Mann–Whitney test in **d** and a two-tailed Wilcoxon matched-pairs singled-rank test in **e**. ANOVA, analysis of variance; NS, not significant.

the circulation and exacerbate the inflammatory response systemically and at distal sites[8,9]. Beyond bacteria, the fungal microbiota (mycobiota) can activate protective or proinflammatory immunity in a context-dependent manner[10]. Fungi are common inhabitants of the human GI tract and can contribute to intestinal, airways and systemic inflammation during pathophysiological conditions[11,12]. Dangerous secondary lung infections with *Aspergillus spp.* and *Mucor spp.* have been reported in critically ill patients with COVID-19 (ref. 13) and changes in intestinal mycobiota composition have been observed in patients with sCOVID-19 (refs. 14,15). Despite these correlations, it is currently unknown whether persistent alterations of intestinal mycobiota in conditions of impaired gut barrier function and prolonged immune activation have an impact on host immunity in sCOVID-19.

Here we demonstrate the contribution of intestinal fungal pathobiont to the immunopathology of sCOVID-19 through the activation of neutrophils and their progenitors. This effect is interleukin-6 (IL-6)-dependent and persists for up to a year after recovery, as indicated by elevated anti-*Candida* antibodies and activation of antifungal immune pathways in granulocyte myeloid progenitors (GMPs). Experiments with *Candida albicans* in mice revealed increased lung neutrophilia and pulmonary NETosis during SARS-CoV-2 infection, which was partially alleviated with antifungal treatment or IL-6 receptor (IL-6R) blockade. These findings underscore the lasting impact of intestinal fungal pathobionts on host immunity and pulmonary inflammation in situations involving ongoing immune alterations and impaired gut barrier function, as seen in sCOVID-19.

Results

sCOVID-19 patients develop antibodies to intestinal fungi

The induction of systemic antifungal immunoglobulin G (IgG) antibodies has been an important readout for immune responses to fungal microbiota during homeostasis or in several immune-mediated diseases[16,17]. Because antibodies against fungal mannan (anti-*Saccharomyces cerevisiae* antibodies (ASCA)) are increased in patients with immune-mediated pathologies targeting the GI tract, such as Crohn's disease (CD)[16,18], we characterized ASCA responses in a cohort

https://doi.org/10.1038/s41590-023-01637-4

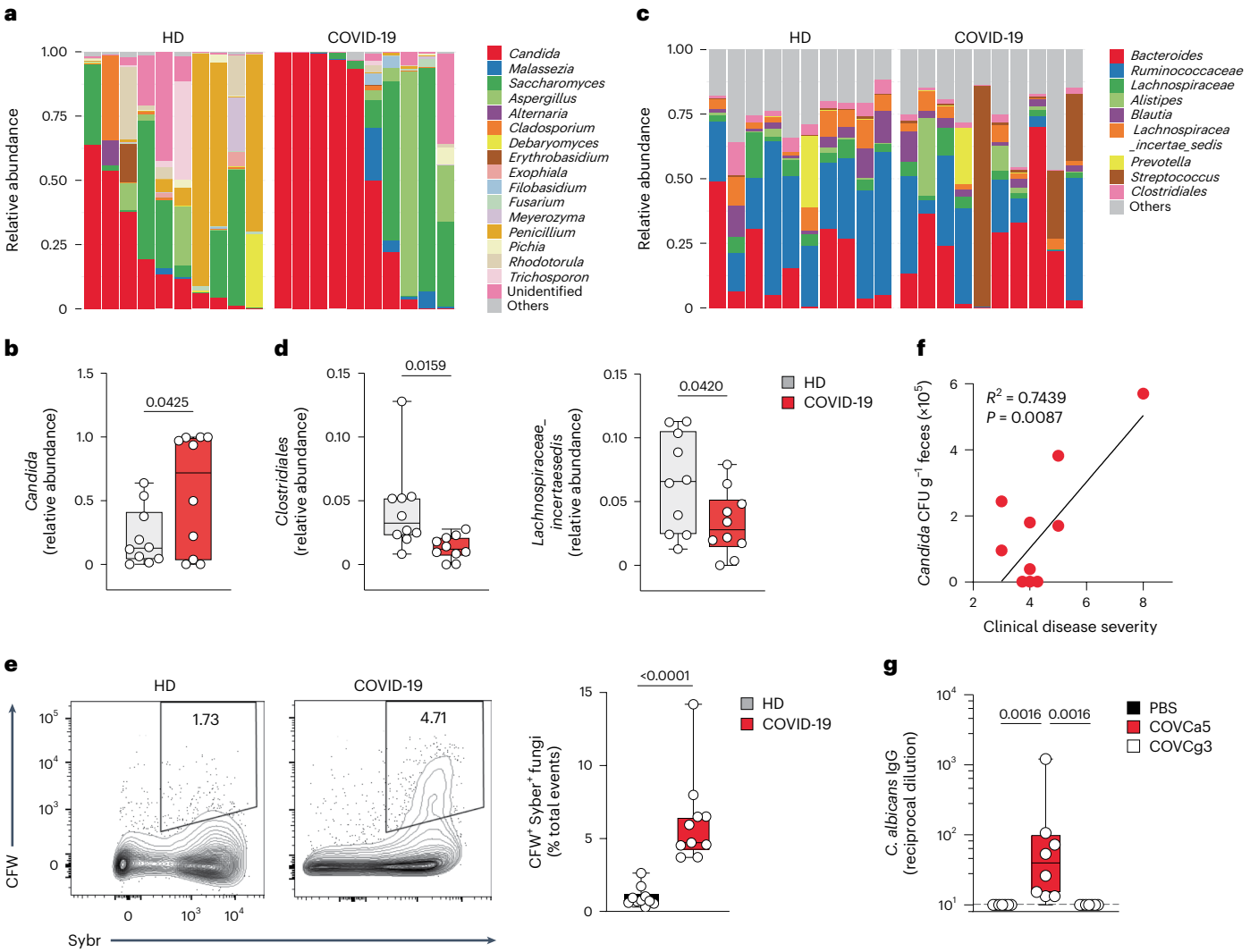

Fig. 2 | *Candida* species of the gut mycobiota expand in sCOVID-19. a, Stack plot of relative abundances of 17 fungal genera with the highest average abundance, assessed by ITS1 sequencing of fungal rDNA from stool samples of HD (n = 10) and sCOVID-19 (n = 10) in cohort 3 (Extended Data Tables 3 and 4). **b**, Relative abundance of *Candida*. **c**, Stack plot of relative abundances of nine bacterial genera with the highest average abundance assessed by 16S sequencing of bacterial rDNA of stool samples as in (**a**). **d**, Relative abundance of *Clostridiales* and *Lachnospiraceae*. Lower and upper hinges (**b** and **d**) correspond to the first and third quartiles. **e**, Representative flow cytometry plots for multi-KAP-based assessment of fungal biomass (CFW^+ $SybrGreen^+$) and the percentage of CFW^+ $SybrGreen^+$ cells per total event from fecal samples of COVID-19 ($n = 10$) and HD ($n = 10$) in cohort 3 (Extended Data Tables 3 and 4). Insets indicate the percentage of cells within the gate in representative plots. **f**, Linear regression analysis of Candida species (CFU g^{-1} of stool) in the stool of patients with COVID-19 (n = 10) and disease severity as defined by an eight-category ordinal scale score (Methods). **g**, *C. albicans* specific IgG titers in the serum of antibiotic-treated mice 2 weeks after oral gavage with either PBS ($n = 7$), *C. albicans* (COVCa5, $n = 8$) or *C. glabrata* (COVCa3, $n = 7$) strains isolated from the stool of patient with COVID-19. The results were pooled from two experiments. For all boxplots, the center is drawn through the median of the measurement, and the lower and upper bounds of the box correspond to the first and third quartiles. The whiskers go down to the smallest value and up to the largest. Dots represent individual patients (**b**,**d**,**e**,**f**) and mice (**g**). *P* values were calculated using a two-tailed Mann–Whitney test in **b**, **d** and **f** and the one-way ANOVA followed by Tukey's multiple comparison in **g**.

(hereafter cohort 1) of patients with COVID-19 treated at Weill Cornell Medicine/NewYork Presbyterian Hospital in March–July 2020, during the first wave of SARS-CoV-2 infections (Extended Data Table 1). We recruited 91 patients with COVID-19, 25 of whom had moderate/mild disease (hereafter mCOVID-19), defined as SARS-CoV-2 infection and <6 l min^{-1} noninvasive supplemental oxygen to maintain $SpO_2 > 92\%$, and 66 with severe disease, defined as requiring oxygen at a flow rate higher than 6 l min^{-1} or by an advanced oxygen delivery device including invasive mechanical ventilation. Thirty-six individuals who were never exposed to the virus and tested negative for antibodies to SARS-CoV-2 spike protein were used as healthy individuals (HD; Extended Data Fig. 1a–c). Serological analysis indicated a significant increase of ASCA IgG in patients with COVID-19 when compared to HD (Fig. 1a), despite no reports of clinical or laboratory evidence of overt fungal superficial or systemic infection in this cohort. The overall increase was comparable to ASCA titers in a cohort of patients with CD (Fig. 1a), suggesting that similar to patients who had a chronic intestinal disease[12,19], patients with COVID-19 developed antibodies to fungi. In CD, ASCA may arise in response to fungal species due to the common presence of mannan in fungal cell walls[16]. To identify fungal antibody targets in patients with COVID-19, we assessed the systemic IgG specificities against fungal species commonly associated with the human gut, oral and skin mucosa, as well as environmental fungal species that can lead to serious lung infections in humans[20]. Because COVID-19 clinical manifestations and fungal immune recognition are characterized by specific cellular, cytokine and humoral profiles[9,21], we also assessed whether fungal antibody profiles

were associated with disease severity. This analysis indicated considerable increases of IgG antibody titers to *C. albicans* (ACAL IgG, 3.70-fold), *C. parapsilosis* (3.96-fold) and *S. cerevisiae* (4.18-fold) in the plasma of patients with sCOVID-19 when compared to HD (Fig. 1b). In contrast, IgG antibodies against fungi that can affect the lung[22] or reside on the skin, such as *Aspergillus, Alternaria* and *Malassezia* species, remained unchanged (Fig. 1c). Intensive care unit (ICU) admission by itself can lead to increased fungal exposure[23]. In five patients admitted to the ICU for diseases not related to COVID-19 (non-COV, cohort 2), we did not observe increased ACAL IgG compared to sCOVID-19 (Extended Data Table 2 and Fig. 1d), suggesting that the increase in ACAL and ASCA titers was not a consequence of ICU admission. This data suggested that antifungal antibodies in patients with COVID-19 were elicited by a specific subset of the gut mycobiota.

To assess whether the high titers of antifungal antibodies were present before SARS-CoV-2 infection or were generated during disease, we assessed samples from a longitudinal sampling collected at clinical diagnosis of infection (V1) and during acute disease (more than 2 weeks after the initial diagnosis, V2) in mCOVID-19 ($n = 6$) and sCOVID-19 ($n = 6$) patients from cohort 1. We found no increase of antifungal antibody titers at V2 in mCOVID-19 compared to those at V1 (Fig. 1e). In contrast, a significant increase of ACAL and ASCA titers was detected at V2 in sCOVID-19 (Fig. 1e). These results indicate that an antibody response to specific fungi developed in sCOVID-19 while such increased antibody titers were not detected before infection.

Gut *Candida* expansion correlates with COVID-19 severity

Gut mycobiota composition has been extensively studied in multiple human cohorts[19,24,25], and internal transcribed spacer (ITS) sequencing analyses have reported gut fungal dysbiosis in a cohort of patients with COVID-19 (refs. 14,15). To address whether SARS-COV-2 infection impacts gut mycobiota, we performed an ITS1-based barcoding approach to deep sequence the ITS1 regions of fungal rDNA from fecal samples collected at the time of hospitalization from ten patients with COVID-19 (cohort 3), of which three had sCOVID-19 and seven had mCOVID-19, as well as from ten HD (Extended Data Table 3). We found that patients with COVID-19 had an increased fungal load in fecal samples compared with uninfected control and that the gut mycobiota was dominated by the Basidiomycota and Ascomycota phyla (Extended Data Fig. 2a), similar to the phyla composition in multiple human cohorts[19,24]. Mycobiota taxonomic composition indicated that *Candida* and *Saccharomyces spp*. were the most common fungal genera detected in both COVID-19 and HD groups (Fig. 2a). Fungal diversity decreased in COVID-19 samples compared to HD, consistent with fungal dysbiosis in patients with COVID-19 (ref. 15). Compared to HD controls, patients with COVID-19 showed an increased relative abundance of fecal *Candida* spp., while the relative abundance of other fungal genera was similar between the two groups (Fig. 2b and Extended Data Fig. 2b). The relative expansion of *Candida* spp. correlated with a decreased relative abundance of anaerobic bacterial genera such as *Clostridiales* and *Lachnospiraceae* (Fig. 2c,d), consistent with other studies exploring transkingdom relations between fungi and bacteria in patients[24,25].

To evaluate whether changes in the relative abundance of *Candida* spp. are due to fungal expansion, we assessed the fungal biomass using a multi-kingdom antibody profiling (mulitKAP) approach[17], which can distinguish fungal from bacterial cells by staining with the fungal cell wall binding dye calcofluor white (CFW). Expansion of the fungal biomass was more prevalent in the gut of patients with COVID-19 compared to HD (Fig. 2e). Based on the results of the ITS sequencing, we developed a culture-based approach to isolate, identify and collect live fungi from fecal samples of mCOVID-19 and sCOVID-19. *C. albicans* was common in the gut of patients with COVID-19 and expanded in the culture from fecal samples of patients with COVID-19 independent of antibiotic therapy (Extended Data Table 4). Notably, *Candida* growth (colony-forming unit (CFU) g^{-1} feces) correlated with disease severity (Fig. 2f), suggesting an association between intestinal overgrowth of *C. albicans* strains and sCOVID-19.

Gut fungal dysbiosis was reported to aggravate disease severity in airway inflammation[11,26]. To test whether specific fungal species in the gut mycobiota have a role in COVID-19 by priming aberrant immunity, we colonized C57BL/6J mice with *Candida* strains isolated from the gut of patients with COVID-19 (hereafter referred to as COVCa). Mice colonized with COVCa for 2 weeks had a significant increase of circulating ACAL antibodies in the blood, while mice colonized with *Candida glabrata* isolated from a patient with COVID-19 (COVCg) did not, compared with noncolonized mice (Fig. 2g and Extended Data Fig. 3a). This finding was confirmed using multiple *C. albicans* (COVCa1, COVCa2 and COVCa5) isolates (Extended Data Fig. 3b). The magnitude of antibody titers induction was dependent on the COVCa strain; titers increased 45.5-, 342.6- and 41.6-fold in COVCa1-, COVCa2- and COVCa5-colonized mice, respectively, compared to noncolonized mice (Extended Data Fig. 3b), as previously reported for gut T helper 17 (T_H17) cell responses in the context of inflammatory bowel disease (IBD)[27], suggesting that the intestinal expansion of *C. albicans* could be responsible for the observed increase of fungal IgG antibodies in the serum of patients with COVID-19 and that ACAL IgG antibodies might serve as a surrogate marker of the host response to intestinal *C. albicans*.

Systemic neutrophilia in sCOVID-19 associates with ACAL IgG levels

Neutrophils have a key role in the development of sCOVID-19 (ref. 28). Increased serum levels of neutrophil-released calprotectin, which associates with the severity of the pathogen-associated tissue damage or with excessive cytokine storm, have been reported in patients with sCOVID-19 (ref. 28). We found increased calprotectin in the plasma of sCOVID-19 compared to HD (Fig. 3a). To assess the general landscape

Fig. 3 | Neutrophils and ACAL IgG differentiate mCOVID-19 from sCOVID-19 and link intestinal *Candida* overgrowth to proinflammatory immunity in the lung. a, Calprotectin plasma levels in HD ($n = 36$), mCOVID-19 ($n = 25$) and sCOVID-19 ($n = 66$) from cohort 1 (Extended Data Table 1). **b**–**d**, Scatter plots of lymphocytes and myeloid cells (**b**) and $Lin^-CD11b^+CD14^+CD15^-$ MO, $Lin^-CD11b^+CD14^-CD15^-$ monocyte-derived cells (MC) and $Lin^-CD11b^+CD14^-CD15^+$ polymorphonuclear neutrophils/granulocytes (PMNs) frequencies (**c**) in the blood (**b**,**c**) and calprotectin levels in the plasma (**d**) against levels of ACAL plasma IgG in sCOVID ($n = 13$) and mCOVID-19 ($n = 17$) from cohort 1 (Extended Data Table 1). Crosses indicate deceased patients. Red and black lines show linear fits within severe and low to moderate groups, respectively, with 95% confidence intervals shown in gray. Spearman correlation estimates (rho) and associated *P* values are shown in red and black for sCOVID-19 and mCOVID-19, respectively. **e**, Representative plots and the number of $CD45^+Ly6G^+CD11b^+$ neutrophils in peripheral blood and lung at week 2 after intestinal colonization of antibiotic-treated mice with either *C. albicans* (COVCa5, $n = 8$) or *C. glabrata* (COVCa3, $n = 7$), or oral gavage with PBS ($n = 7$). Insets indicate the percentage of cells within the gate. The results were pooled from two experiments. **f**, Serum calprotectin and the number of $Ly6G^+CD11b^+$ neutrophils in peripheral blood and lung at week 2 in mice that received oral gavage with PBS ($n = 5$), COVCa5 ($n = 5$) or COVCa5 followed by treatment with fluconazole 2 d after COVCa5 colonization (COVCa5 + fluconazole, $n = 5$). Data in **f** are representative of two experiments. For boxplots in **a**, the center is drawn through the median of the measurement, and the lower and upper bounds of the box correspond to the first and third quartiles. The whiskers go down to the smallest value and up to the largest. The bar graphs are presented as mean ± s.e.m. Plots represent individual patients (**a**–**d**) and mice (**e**,**f**). Correlation analysis in **b**–**d** was assessed using the Spearman correlation coefficient with a two-tailed test. Differing correlations between severe versus mild/moderate groups were assessed by evaluating the significance of an interaction. *P* values were calculated using the one-way ANOVA followed by Tukey's multiple comparison in **a** and Kruskal–Wallis test with Dunn's post hoc test in **e** and **f**.

https://doi.org/10.1038/s41590-023-01637-4

of immune response during COVID-19, we performed extensive immunophenotyping to characterize the frequency of circulating immune subsets in 30 patients (17 mCOVID-19 and 13 sCOVID-19) from cohort 1 (Extended Data Table 1)[29]. Flow-cytometry-based immune cell profiling of peripheral blood showed a strong correlation between the presence of ACAL IgG and frequency of Lin$^-$CD11b$^+$CD33$^+$ myeloid cell in sCOVID-19, but not in mCOVID-19 (Fig. 3b; linear regression with interaction term, $P = 0.005$). There was no correlation between ACAL IgG and the lymphoid compartment (Fig. 3b; interaction $P = 0.117$) or specific populations of lymphocytes such as CD3$^-$CD56$^+$CD16$^+$NK cells, CD3$^+$CD4$^+$ T cells, CD3$^+$CD8$^+$ T cells and CD19$^+$B220$^+$ B cells (Extended Data Fig. 4a–e). We observed a global loss of lymphocytes among CD45$^+$ cells and an enrichment of the myeloid cell compartment in the peripheral blood of sCOVID-19 compared to mCOVID-19 or HD (Fig. 3c), consistent with other reports[30]. Deeper analysis showed that a population of Lin$^-$CD11b$^+$CD16$^+$CD14$^-$CD15$^+$ polymorphonuclear neutrophils/

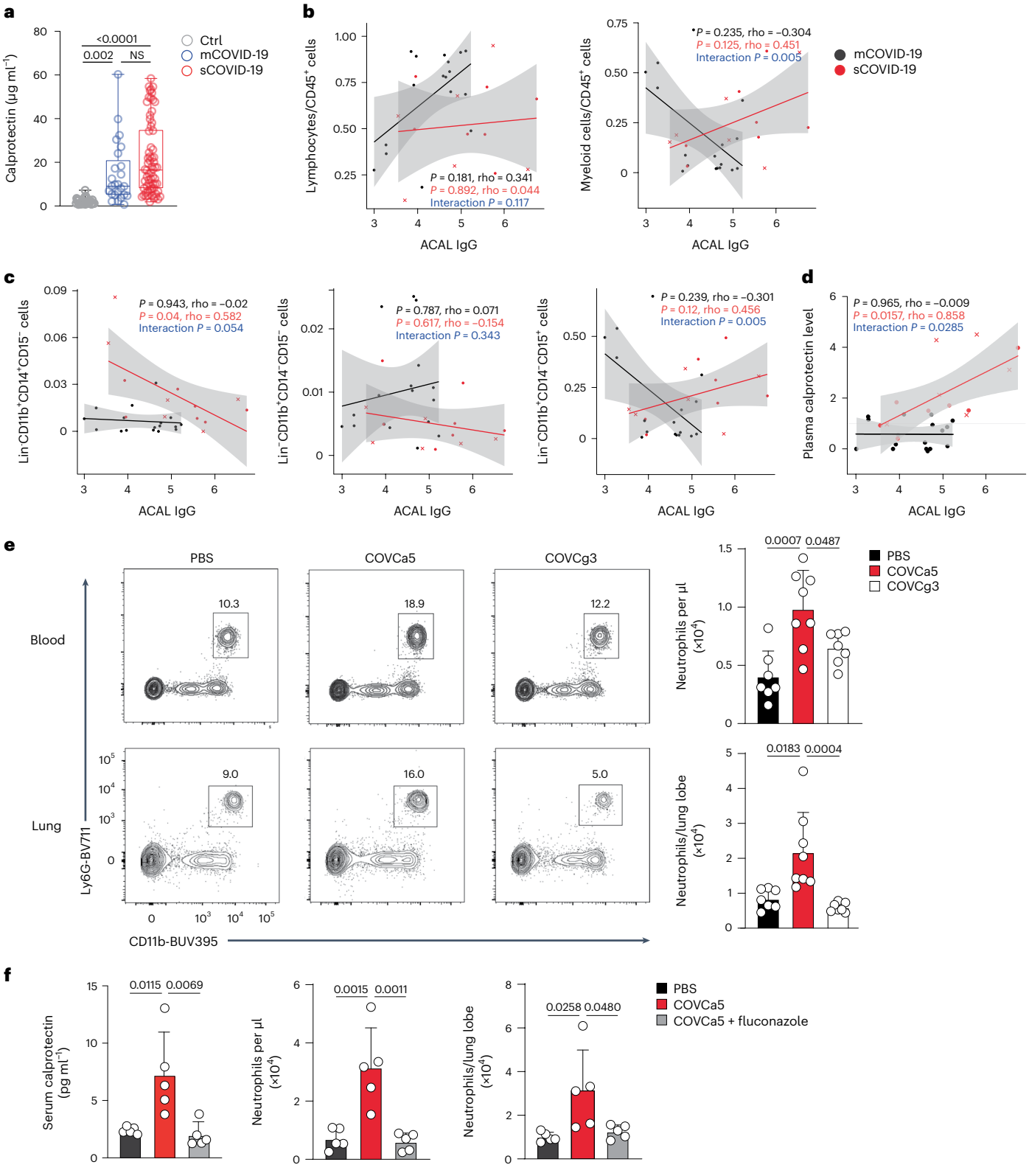

granulocytes (PMNs), but not Lin$^-$CD11b$^+$CD16$^+$CD14$^+$CD15$^+$ monocytes (MO) and Lin$^-$CD11b$^+$CD16$^+$CD14$^-$CD15$^+$ MO-derived cells, was responsible for this signal (Fig. 3c). These findings were corroborated by positive correlation between ACAL IgG and plasma calprotectin levels in peripheral blood (Fig. 3d). Neutrophils can be induced by intestinal colonization with laboratory strain of *C. albicans*[31]. Immune cell profiling of peripheral blood and lungs from COVCa5-colonized, COVCg3-colonized or noncolonized mice (Extended Data Fig. 3c) showed that intestinal colonization with COVCa5, but not with COVCg3, led to an increased frequency and absolute numbers of circulating Ly-6G$^+$CD11b$^+$ neutrophils in the blood and the lungs of mice 2 weeks after colonization compared to those of noncolonized and COVCg3-colonized mice (Extended Data Fig. 3c,d). Notably, treatment with the antifungal drug fluconazole dampened the number of Ly-6G$^+$CD11b$^+$ neutrophils in the blood and lung of COVCa5-colonized mice and reduced the expression of calprotectin in the serum compared to noncolonized mice (Fig. 3e,f). This data suggested that the increase in intestinal *C. albicans* correlated with the frequency of polymorphonuclear neutrophils and the level of the inflammatory marker calprotectin in sCOVID-19.

Altered GMP function persists after sCOVID-19 recovery

Many patients who have recovered from acute COVID-19 infection experience persistent or new symptoms for 4 weeks or more following the initial SARS-CoV-2 infection[32], which leads to significant disability and impairment of normal daily life. PASC is suspected to be in part related to aberrant cellular or humoral immune responses to self- and microbiota-derived antigens. To identify mycobiota-related immune features in patients with COVID-19, we collected convalescent plasma and peripheral blood mononuclear cells (PBMCs) samples at months 2–4 postdisease onset (early recovery) or months 4–12 (late recovery) from patients in cohort 2 (Extended Data Table 2), who were monitored in ICU for 2–4 months as intermediate care until discharged, and then seen as out-patients in the post-ICU clinic for 4–12 months. In cohort 2, we assessed plasma antibody titer against fungi and expression of calprotectin in mCOVID-19 (early recovery, $n = 7$; late recovery, $n = 5$), sCOVID-19 (early recovery, $n = 10$; late recovery, $n = 14$) and HD ($n = 8$). Higher levels of ACAL antibodies were detected in convalescent patients who had experienced severe disease compared to those with mCOVID-19 or HD at early recovery, and high ACAL levels persisted for up to 12 months (last time point we measured; Fig. 4a). On the other hand, the titers of antibodies against *Aspergillus fumigatus* and bacterial flagellin were similar across all groups (Fig. 4a). This data suggested a lasting antifungal antibody signature in patients recovering from sCOVID-19.

Increased numbers of circulating neutrophils with an inflammatory phenotype have been reported in patients with sCOVID-19 with persistent pulmonary symptoms 3–6 months postdisease onset[33]. Calprotectin levels, which were assessed as a proxy of the frequency of circulating neutrophils, were elevated at months 2–4 postdisease onset, but significantly declined at months 4–12 in patients with sCOVID-19 (Fig. 4b), suggesting that neutrophils returned to pre-sCOVID-19 levels during late recovery. Altered immune cell composition, neutrophil function and hematopoiesis that persists months after infection have been reported in patients with sCOVID-19 (refs. 33,34). To determine whether sCOVID-19 induced changes in the hematopoietic stem and progenitor cells (HSPC) compartment that were retained during convalescence, we enriched CD34$^+$ HSPC from the PBMC of HD ($n = 5$), sCOVID-19 ($n = 12$) and non-COV ($n = 5$) patients from cohort 2 and performed scRNA-seq. We acquired 28,069 peripheral CD34$^+$ HSPC and identify differentially expressed genes among the ten resulting subclusters[34] after preprocessing and cell-type annotation (Fig. 4c). HSPC subsets were manually annotated as hematopoietic stem cells and multipotent progenitors (HSC/MPP), lymphoid-primed MPP, megakaryocyte–erythroid progenitors, erythroid progenitors, granulocyte monocyte progenitors (GMP) and basophil–eosinophil–mast cell progenitors based on the marker gene expression[34] (Fig. 4c). We detected increased transcription of genes encoding C-type lectin receptors (*CLEC7A, CLEC6A* and *CLEC4E*), downstream signaling molecules (*MALT1, SYK, BAK1* and *BTK*) and Toll-like receptor 2 in CD34$^+$ HPSCs from sCOVID-19 compared with HD (Fig. 4d). Increased frequency of GMPs was observed in early and late recovery sCOVID-19 (Fig. 4e) and positively associated with ACAL IgG titers from convalescent plasma (Fig. 4f and Extended Data Fig. 5). Furthermore, GMP from sCOVID-19 had high expression of myeloperoxidase (*MPO*) and *ELANE* genes, which encode for neutrophil granule proteins MPO and elastases, compared to HD (Fig. 4g). Together, these observations suggested that gut commensal fungal opportunists such as *C. albicans* might contribute to long-lasting alterations in neutrophil progenitors associated with prolonged COVID-19.

C. albicans affects IL-6R-dependent GMP activation and lung NETosis

Assessment of multiple cytokines in mice intestinally colonized with mucosa-associated fungi, including *C. albicans* showed an increase of IL-6 in the serum[35]. Because gut *C. albicans* can affect systemic immunity[11,17,31] and neuronal function through cytokine-mediated mechanisms[35], we tested whether *C. albicans*-induced IL-6R contributed to the induction of neutrophilia. C57BL/6J mice colonized with COVCa5 showed a significant increase in blood circulating Ly-6G$^+$CD11b$^+$ neutrophils and ACAL antibodies 2 weeks after colonization, whereas COVCa5-colonized mice treated intraperitoneally with IL-6R neutralizing antibodies the day before colonization showed a decrease in ACAL antibodies in the serum and a decrease in the frequency of Ly-6G$^+$CD11b$^+$ neutrophils in peripheral blood and the lung 2 weeks post-COVCa5

Fig. 4 | Persistently altered function of neutrophil progenitors in patients recovering from sCOVID-19. a,**b**, Plasma IgG antibody titers to *C. albicans* (ACAL IgG), *A. fumigatus* and flagellin (**a**) or calprotectin levels (**b**) in HD ($n = 8$) and patients recovering from mCOVID-19 (months 2–4, $n = 7$), mCOVID-19 (months 4–12, $n = 5$), sCOVID-19 (months 2–4, $n = 10$) and sCOVID-19 (months 4–12, $n = 18$; Extended Data Table 2). **c**, Subject-paired analysis of PBMCs (left) and hematopoietic stem and progenitor cells (HSPC) subsets (right) with enrichment of CD34$^+$ HSPC from PBMC followed by combined single-nuclei RNA-seq/ATAC-seq (multiome). Plots in PBMC were annotated for major immune cell types; B cells, CD14$^+$ and CD16$^+$ monocytes, CD4$^+$ and CD8$^+$ T cells, dendritic cells (DC), HSPC, natural killer cells (NK), plasma B cell (PC) and plasmacytoid dendritic cells (pDC). Plots in HSPC were annotated for major progenitor cell types; erythroid progenitor cells (Ery), basophil–eosinophil–mast cell progenitor cells (BEM), lymphoid-primed multipotent progenitor cells (LMPP), megakaryocyte–erythroid progenitor cells (MEP), HSC/MPP and granulocyte–macrophage progenitor cells (GMP). **d**, Heatmap representation of differentially expressed genes involved in antifungal immunity and signaling by HSPC from HD ($n = 5$) and sCOVID-19 ($n = 12$). **e**, Boxplots representing the frequency of GMPs in enriched CD34$^+$ HSPC from HD ($n = 5$) and sCOVID-19 ($n = 12$). The data in **e** and **f** represent normalized expression by sctranform[34]. **f**, Correlation and linear regression of antifungal (*C. albicans* or *A. fumigatus*) or antibacterial (flagellin) IgG antibodies ($\log_{10}$ titer) or calprotectin levels ($\log_{10}$ concentration) with frequency of GMP. Each dot represents HD ($n = 5$), sCOVID ($n = 12$) and non-COV ($n = 5$). Blue line indicates the regression line for all patients. The associated linear regression equation, Pearson's correlation. Coefficient and significance are shown. **g**, Violin plots showing the distribution of MPO expression in GMPs at months 2–4 ($n = 4$) and months 4–12 ($n = 8$) posthospital admission of sCOVID-19 versus HD ($n = 5$). For boxplots in **a**, **b** and **e**, the center is drawn through the median of the measurement, and the lower and upper bounds of the box correspond to the first and third quartiles. The whiskers go down to the smallest value and up to the largest. Dots represent individual patients (**a**,**b**,**e**,**f**) and cells (**g**). *P* values were calculated using the one-way ANOVA followed by Tukey's multiple comparison in **a** and **b**; Pearson's correlation in **f** and a two-tailed Mann–Whitney test in **e** and Kruskal–Wallis test with a Dunn's post hoc test in **g**.

https://doi.org/10.1038/s41590-023-01637-4

colonization compared to COVCa5-colonized mice without IL-6R neutralizing antibodies (Fig. 5a–c).

Administration of tocilizumab, a monoclonal antibody against the IL-6R, to patients with sCOVID-19 was reported to be either beneficial or neutral on disease outcome depending on the study design[36]. We collected blood samples from cohort 2 sCOVID-19 patients who received tocilizumab during the acute phase of the disease ($n = 10$) and analyzed that data against patients who did not receive the drug ($n = 7$). The administration of tocilizumab in cohort 2 was nearly random during the 2020 COVID-19 peak in New York City, therefore no apparent clinical or demographic features influenced the analyses. Although we were unable to analyze the number of intact neutrophils in these samples, ACAL antibody titers (Fig. 5d), but not flagellin antibodies (Fig. 5d), were reduced in the convalescent plasma of tocilizumab-treated

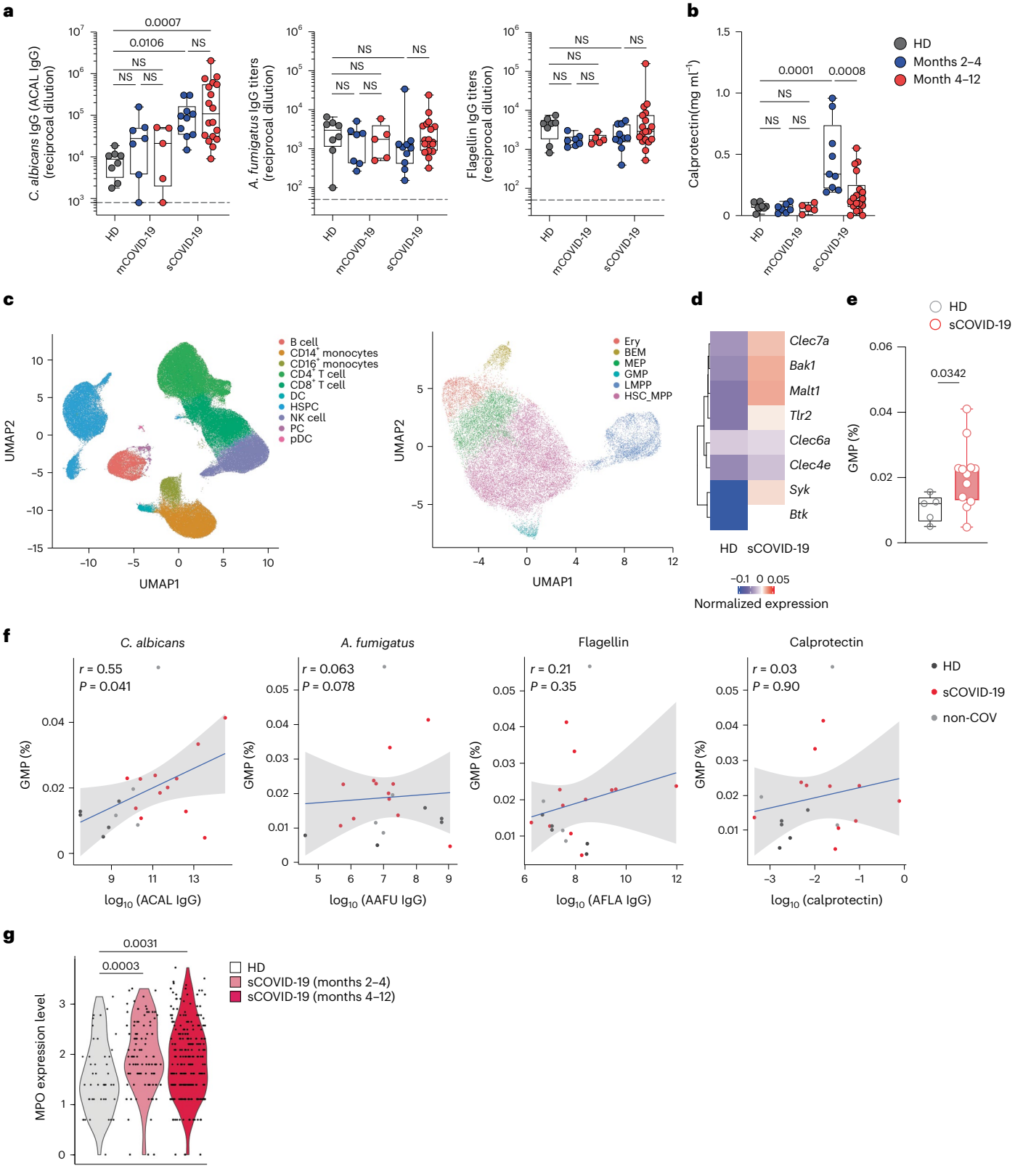

https://doi.org/10.1038/s41590-023-01637-4

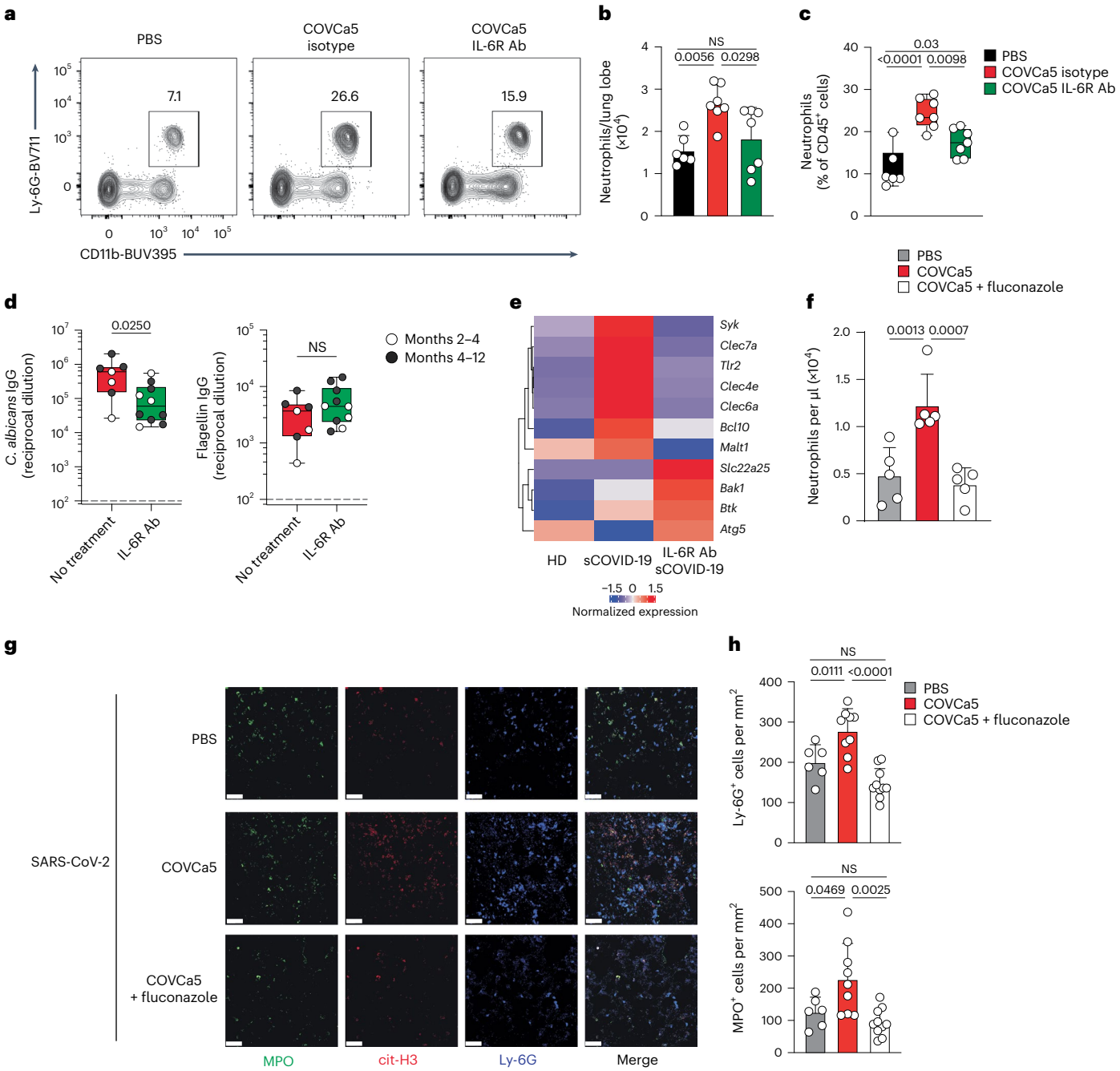

Fig. 5 | IL-6 mediates immune activation in patients with severe COVID-19 and in a mouse model of COVID-19 during *C. albicans*-aggravated lung NETosis. **a**, Representative dot plots of lung CD45$^+$CD11b$^+$Ly-6G$^+$ neutrophils from COVCa5-colonized mice treated with IL-6R ($n = 7$) or isotype ($n = 7$) antibodies every other day for 2 weeks postcolonization or were left uncolonized and untreated (PBS, $n = 6$). Insets indicate the percentage of cells within the gate. **b**,**c**, Absolute numbers and percentage of CD45$^+$CD11b$^+$Ly-6G$^+$ neutrophils in lung CD45$^+$ cells, as in **a**. **d**, Plasma IgG antibody titers to *C. albicans* and flagellin in patients with sCOVID-19 (months 2–4) and sCOVID-19 (months 4–12) who received IL-6R blockade treatment during acute infection (IL-6R Ab, $n = 10$) or not (no treatment, $n = 7$). The results were pooled from two experiments. **e**, Heatmap of genes involved in fungal recognition in blood GMPs isolated from sCOVID-19 who received IL-6R blockade treatment (IL-6R Ab sCOVID, $n = 6$) or not (sCOVID, $n = 7$) during acute COVID-19 infection or from HD ($n = 7$). **f**–**h**, Number of Ly6G$^+$CD11b$^+$ cells in the peripheral blood as assessed by flow cytometry (**f**) and immunofluorescence images (**g**) and quantification (**h**) of H3Cit$^+$, MPO$^+$ and Ly-6G$^+$ neutrophils from multiple fields (20×) of lung sections (**g**,**h**) at day 5 postintranasal inoculation with SARS-COV-2 in mice that were uncolonized (PBS, $n = 5$) or colonized with COVCa5 at day 14 before infection (Extended Data Figure 6b) and left untreated ($n = 5$) or treated with fluconazole ($n = 5$) 2 d after colonization for the duration of the experiment. White scale bar (**g**) indicates 30 µm. Image analysis was conducted on acquired images as follows: two slides per animal of $n = 3$–5 animals. The data are representative of two experiments. For boxplots in **c** and **d**, the center is drawn through the median of the measurement, and the lower and upper bounds of the box correspond to the first and third quartiles. The whiskers go down to the smallest value and up to the largest. The bar graphs in **b**, **f** and **h** presented as mean ± s.e.m. Dots represent individual patients (**d**) and mice (**b**,**c**,**f**,**h**). *P* values were calculated using the one-way ANOVA followed by Tukey's multiple-comparison in **b**, **c**, **f** and **h** and a two-tailed Mann–Whitney test in **d**.

patients with COVID-19 compared with patients who did not receive tocilizumab treatment. Notably, the increased transcription of genes encoding C-type lectin receptors (*CLEC7A, CLEC6A* and *CLEC4E*), downstream signaling molecules (*BCL10, MALT1, SYK, BAK1* and *BTK*) and antigen presentation (*HLA-B*, *HLA-DQ*, *CD74*, *B2M* and *IFI30*) was decreased in GMPs from recovering tocilizumab-treated patients compared to those without treatment (Fig. 5e and Extended Data Fig. 6a), suggesting that targeting the IL-6 pathway during sCOVID-19 had a positive impact on GMP transcriptional signatures and the decrease of ACAL titers. Together, this data indicated that IL-6 was a key mediator of the systemic immune effects exerted by gut *C. albicans* and might contribute to the immunopathology of sCOVID-19.

Interstitial lung changes in the acute stage of COVID-19 are associated with increased systemic neutrophils and markers of neutrophil extracellular trap (NET) formation, suggesting a potential role for neutrophils in sCOVID-19 and potentially long COVID[33,37]. To assess whether intestinal fungi could influence the hyperinflammation in the lung in sCOVID-19, we used aged mice as a model of disease[38]. Twelve months old 129S1/SvImJ colonized with COVCa5 2 weeks before infection with SARS-CoV-2 (Extended Data Fig. 6b) showed a significant increase of neutrophils in the peripheral blood 5 d post-SARS-CoV-2 infection compared to SARS-CoV-2-infected, non-COVCa5-colonized mice (Fig. 5f). Furthermore, mature pulmonary Ly-6G$^+$CD11b$^+$ neutrophils that were MPO$^+$ and produced NETs were observed more frequently in the lung of COVCa5-colonized mice that were infected with SARS-CoV-2 compared to non-COVCa5-colonized, SARS-CoV-2-infected mice (Fig. 5g,h). Antifungal treatment with fluconazole (which targeted intestinal COVCa5), starting at day 2 post-COVCa5 colonization for the duration of the experiment, decreased the numbers of circulating Ly-6G$^+$CD11b$^+$ neutrophil and NET formation in the lung compared to those of COVCa5-colonized mice without fluconazole (Fig. 5f–h). This finding aligns with current data in patients with candidemia[39]. This data suggested that expansion of gut *C. albicans* in patients with sCOVID-19 could modulate neutrophil numbers and function in the blood and lungs.

Discussion

Here we report that in addition to devastating secondary fungal infections in patients with severe pulmonary dysfunction[40], the mycobiota of the GI tract might be a contributing factor to the immunopathology of sCOVID-19. High-resolution ITS1-based sequencing survey, multi-KAP and culture-dependent analysis indicated the presence of *C. albicans* in fecal samples from patients with COVID-19. Antifungal IgG antibody repertoire exploration detected increased titers of systemic IgG antibodies against *C. albicans* and other fungi associated with the GI tract, but not toward commonly inhaled fungi, in patients with sCOVID-19. The analysis of HSC progenitors in patients with sCOVID-19 showed transcriptional alterations in pathways related to antifungal immunity and lasting reprogramming of GMPs, which were partially resolved upon targeting the IL-6 pathway with the drug tocilizumab. Mice colonized with *C. albicans* strains from patients with COVID-19 experienced increased ACAL IgG as well as lung neutrophilia and pulmonary NETosis during infection with SARS-CoV-2, which were partially resolved by antifungal treatment and by the blockade of IL-6.

A growing body of literature has reported how immune cell dysfunction contributes to the inflammatory response in patients with sCOVID-19 (ref. 41), with microbiome-related factors also contributing to COVID-19 severity[42]. Our data suggested that the gut mycobiota could have a role in modulating the host immune response and could induce lasting immune alterations in the antifungal antibody response and the HSC compartment in patients with COVID-19 .

We observed that mature Ly-6G$^+$CD11b$^+$ neutrophils in the lungs of SARS-CoV-2-infected mice that were previously colonized with *C. albicans* exhibited enhanced production of MPO and enhanced release of NETs compared to the SARS-Cov-2-infected, non-*C. albicans*-colonized mice. These observations suggested that *C. albicans* had an additional impact on neutrophils that amplified the detrimental effect of SARS-CoV-2 infection. This amplifying effect could be explained by the induction of fungal sepsis and/or the increased activation, maturation and overall numbers of neutrophils and their progenitors by fungal pathogen-associated molecular patterns (PAMPs). Fungal sepsis was reported in patients with sCOVID-19 with an incidence of 1.6–4.4%[39,43]. Fungal PAMPs can enter the circulation during instance of gut barrier disturbance[9,44] and could potentially contribute to neutrophilia in severe cases of COVID-19, where the gut barrier function is compromised[45]. Hence, our findings suggest that gut-colonizing *C. albicans*, through cell or fungal PAMPs translocation, could induce or amplify emergency hematopoiesis, reprogram GMPs and amplify the production of activated neutrophils, which could infiltrate the lungs and contribute to the severity of COVID-19. These findings are further supported by a recent study reporting an expansion of myeloid progenitors in the bone marrow of mice after intestinal colonization with *C. albicans*[46]. Similar mechanisms might be involved in other lung diseases, in which gut-activated fungal antigen-specific T_H17 cells have been observed in the lungs[11].

We showed that treatment with the antifungal drug fluconazole, which targeted intestinal *C. albicans*, reduced the number of circulating Ly-6G$^+$CD11b$^+$ neutrophils and inhibited NET formation in the lungs of COVCa5-colonized mice. This observation was consistent with reports indicating a potential therapeutic benefit of antifungal treatment in patients with COVID-19 with candidemia[39] and underscored the modulatory effect of gut-colonizing *C. albicans* on neutrophil numbers and function. These observations could have implications regarding the potential therapeutic value of antifungal treatment, although future clinical studies are needed to determine causality.

IL-6 is a pleiotropic cytokine with a variety of roles in the immune system that has been linked to tissue damage and immune cell activation in sCOVID-19 (refs. 34,47). Specifically, we found that systemic and lung neutrophilia prompted by intestinal *C. albicans* expansion was dependent on IL-6R. Myeloid signatures and increased numbers of circulating neutrophils in patients with COVID-19 with severe respiratory disease are associated with NET formation and overall worse disease outcomes[48]. NETosis has been shown to contribute to tissue damage in pathophysiological conditions such as systemic lupus erythematosus and rheumatoid arthritis[49]. We found that the expansion of *C. albicans* in the intestine may contribute to the increase in lung neutrophil infiltration and NETosis in mice infected with SARS-CoV-2. Treatment of patients with sCOVID-19 with an IL-6R blocking antibody led to a significant decrease in ACAL IgG and modulated the GMP expression of genes involved in antifungal immunity, which persisted for up to a year post-IL-6R antibody treatment. This suggested that IL-6 may be involved in the long-lasting immune outcomes of post-COVID-19 inflammation, where gut fungi may also have a role. Our findings are consistent with the pleiotropic function of IL-6 on multiple cell types, including B cells, T cells, neutrophils and HSC progenitors[34,50] and highlight the involvement of intestinal *C. albicans* blooms in the pathobiology of both local and systemic inflammation.

Altogether, our findings highlighted a mechanism by which gut fungal pathobionts might contribute to lasting immune alterations during inflammatory diseases and reprogramming of bone marrow progenitors and suggest the potential of mycobiota-immuno-based approaches to identify patients at risk for sCOVID-19 and long-lasting immune alterations.

Online content

Any methods, additional references, Nature Portfolio reporting summaries, source data, extended data, supplementary information, acknowledgements, peer review information; details of author contributions and competing interests; and statements of data and code availability are available at https://doi.org/10.1038/s41590-023-01637-4.

References

1. COVID-19 Dashboard. *The Center for Systems Science and Engineering (CSSE)* (Johns Hopkins University (JHU)) https://coronavirus.jhu.edu/map.html (2023)
2. Guan, W.-J. et al. Clinical characteristics of coronavirus disease 2019 in China. *N. Engl. J. Med* **382**, 1708–1720 (2020).
3. Al-Aly, Z., Bowe, B. & Xie, Y. Long COVID after breakthrough SARS-CoV-2 infection. *Nat. Med.* **28**, 1461–1467 (2022).
4. Lucas, C. et al. Longitudinal analyses reveal immunological misfiring in severe COVID-19. *Nature* **584**, 463–469 (2020).
5. Lau, R. I. et al. Gut microbiota in COVID-19: key microbial changes, potential mechanisms and clinical applications. *Nat. Rev. Gastroenterol. Hepatol.* **20**, 323–337 (2023).
6. Miyauchi, E., Shimokawa, C., Steimle, A., Desai, M. S. & Ohno, H. The impact of the gut microbiome on extra-intestinal autoimmune diseases. *Nat. Rev. Immunol.* **23**, 9–23 (2023).
7. Hou, K. et al. Microbiota in health and diseases. *Signal Transduct. Target. Ther.* **7**, 135 (2022).
8. Liu, Q. et al. Multi-kingdom gut microbiota analyses define COVID-19 severity and post-acute COVID-19 syndrome. *Nat. Commun.* **13**, 6806 (2022).
9. Arunachalam, P. S. et al. Systems biological assessment of immunity to mild versus severe COVID-19 infection in humans. *Science* **369**, 1210–1220 (2020).
10. Li, X. V., Leonardi, I. & Iliev, I. D. Gut mycobiota in immunity and inflammatory disease. *Immunity* **50**, 1365–1379 (2019).
11. Bacher, P. et al. Human anti-fungal Th17 immunity and pathology rely on cross-reactivity against *Candida albicans*. *Cell* **176**, 1340–1355 (2019).
12. Leonardi, I. et al. CX3CR1^{+} mononuclear phagocytes control immunity to intestinal fungi. *Science* **359**, 232–236 (2018).
13. Salmanton-García, J. et al. COVID-19-associated pulmonary aspergillosis, March–August 2020. *Emerg. Infect. Dis. J.* **27**, 1077 (2021).
14. Zuo, T. et al. Alterations in fecal fungal microbiome of patients with COVID-19 during time of hospitalization until discharge. *Gastroenterology* **159**, 1302–1310.e1305 (2020).
15. Lv, L. et al. Gut mycobiota alterations in patients with COVID-19 and H1N1 infections and their associations with clinical features. *Commun. Biol.* **4**, 480 (2021).
16. Standaert–Vitse, A. et al. *Candida albicans* is an immunogen for anti *Saccharomyces cerevisiae* antibody markers of Crohn's disease. *Gastroenterology* **130**, 1764–1775 (2006).
17. Doron, I. et al. Human gut mycobiota tune immunity via CARD9-dependent induction of anti-fungal IgG antibodies. *Cell* **184**, 1017–1031 (2021).
18. Wang, Z. Z., Shi, K. & Peng, J. Serologic testing of a panel of five antibodies in inflammatory bowel diseases: diagnostic value and correlation with disease phenotype. *Biomed. Rep.* **6**, 401–410 (2017).
19. Sokol, H. et al. Fungal microbiota dysbiosis in IBD. *Gut* **66**, 1039–1048 (2017).
20. Brown, G. D. et al. Hidden killers: human fungal infections. *Sci. Transl. Med.* **4**, 165rv113 (2012).
21. Koutsakos, M. et al. Integrated immune dynamics define correlates of COVID-19 severity and antibody responses. *Cell Rep. Med.* **2**, 100208 (2021).
22. Hoenigl, M. et al. COVID-19-associated fungal infections. *Nat. Microbiol.* **7**, 1127–1140 (2022).
23. Proctor, D. M. et al. Integrated genomic, epidemiologic investigation of *Candida auris* skin colonization in a skilled nursing facility. *Nat. Med.* **27**, 1401–1409 (2021).
24. Leonardi, I. et al. Fungal trans-kingdom dynamics linked to responsiveness to fecal microbiota transplantation (FMT) therapy in ulcerative colitis. *Cell Host Microbe* **27**, 823–829 (2020).
25. Zhai, B. et al. High-resolution mycobiota analysis reveals dynamic intestinal translocation preceding invasive candidiasis. *Nat. Med.* **26**, 59–64 (2020).
26. Li, X. et al. Response to fungal dysbiosis by gut-resident CX3CR1^{+} mononuclear phagocytes aggravates allergic airway disease. *Cell Host Microbe* **24**, 847–856 (2018).
27. Li, X. V. et al. Immune regulation by fungal strain diversity in inflammatory bowel disease. *Nature* **603**, 672–678 (2022).
28. Silvin, A. et al. Elevated calprotectin and abnormal myeloid cell subsets discriminate severe from mild COVID-19. *Cell* **182**, 1401–1418 (2020).
29. Rendeiro, A. F. et al. Profiling of immune dysfunction in COVID-19 patients allows early prediction of disease progression. *Life Sci. Alliance* **4**, e202000955 (2021).
30. Mann, E. R. et al. Longitudinal immune profiling reveals key myeloid signatures associated with COVID-19. *Sci. Immunol.* **5**, eabd6197 (2020).
31. Shao, T. Y. et al. Commensal *Candida albicans* positively calibrates systemic Th17 immunological responses. *Cell Host Microbe* **25**, 404–417 (2019).
32. Al-Aly, Z., Xie, Y. & Bowe, B. High-dimensional characterization of post-acute sequelae of COVID-19. *Nature* **594**, 259–264 (2021).
33. George, P. M. et al. A persistent neutrophil-associated immune signature characterizes post-COVID-19 pulmonary sequelae. *Sci. Transl. Med.* **14**, eabo5795 (2022).
34. Cheong, J.-G. et al. Epigenetic memory of coronavirus infection in innate immune cells and their progenitors. *Cell* **186**, 3882–3902 (2023).
35. Leonardi, I. et al. Mucosal fungi promote gut barrier function and social behavior via type 17 immunity. *Cell* **185**, 831–846 (2022).
36. Rosas, I. O. et al. Tocilizumab in hospitalized patients with severe COVID-19 pneumonia. *N. Engl. J. Med.* **384**, 1503–1516 (2021).
37. Zuo, Y. et al. Neutrophil extracellular traps in COVID-19. *JCI Insight* **5**, e138999 (2020).
38. Dinnon, K. H. et al. A mouse-adapted model of SARS-CoV-2 to test COVID-19 countermeasures. *Nature* **586**, 560–566 (2020).
39. Çavuş, M. A. & Sav, H. Opportunistic infections in critical COVID-19 patients. *Pol. J. Microbiol.* **71**, 411–419 (2022).
40. Hoenigl, M. et al. The emergence of COVID-19 associated mucormycosis: a review of cases from 18 countries. *Lancet Microbe* **3**, e543–e552 (2022).
41. Bastard, P. et al. Autoantibodies against type I IFNs in patients with life-threatening COVID-19. *Science* **370**, eabd4585 (2020).
42. Yeoh, Y. K. et al. Gut microbiota composition reflects disease severity and dysfunctional immune responses in patients with COVID-19. *Gut* **70**, 698–706 (2021).
43. Kayaaslan, B. et al. Incidence and risk factors for COVID-19 associated candidemia (CAC) in ICU patients. *Mycoses* **65**, 508–516 (2022).
44. Giron, L. B. et al. Markers of fungal translocation are elevated during post-acute sequelae of SARS-CoV-2 and induce NF-κB signaling. *JCI Insight* **7**, e160989 (2022).
45. Sun, Z. et al. Gut microbiome alterations and gut barrier dysfunction are associated with host immune homeostasis in COVID-19 patients. *BMC Med.* **20**, 24 (2022).
46. Chen, Y.-H. et al. Rewilding of laboratory mice enhances granulopoiesis and immunity through intestinal fungal colonization. *Sci. Immunol.* **8**, eadd6910 (2023).
47. McGonagle, D., Sharif, K., O'Regan, A. & Bridgewood, C. The role of cytokines including interleukin-6 in COVID-19 induced pneumonia and macrophage activation syndrome-like disease. *Autoimmun. Rev.* **19**, 102537 (2020).
48. Veras, F. P. et al. SARS-CoV-2–triggered neutrophil extracellular traps mediate COVID-19 pathology. *J. Exp. Med.* **217**, e20201129 (2020).

49. Wigerblad, G. & Kaplan, M. J. Neutrophil extracellular traps in systemic autoimmune and autoinflammatory diseases. *Nat. Rev. Immunol.* **23**, 274–288 (2023).
50. Tanaka, T., Narazaki, M. & Kishimoto, T. IL-6 in inflammation, immunity, and disease. *Cold. Spring Harb. Perspect. Biol.* **6**, a016295 (2014).

[1]Joan and Sanford I. Weill Department of Medicine, Weill Cornell Medicine, New York City, NY, USA. [2]The Jill Roberts Institute for Research in Inflammatory Bowel Disease (JRI), Weill Cornell Medicine, New York City, NY, USA. [3]Immunology and Microbial Pathogenesis Program, Weill Cornell Graduate School of Medical Sciences, Weill Cornell Medicine, Cornell University, New York City, NY, USA. [4]Department of Pathology and Laboratory Medicine, Weill Cornell Medicine, New York City, NY, USA. [5]Department of Microbiology, Icahn School of Medicine at Mount Sinai, New York City, NY, USA. [6]Global Health and Emerging Pathogens Institute, Icahn School of Medicine at Mount Sinai, New York City, NY, USA. [7]Department of Microbiology, New York University, Langone Health, New York City, NY, USA. [8]Department of Pediatrics, Weill Cornell Medicine, New York City, NY, USA. [9]Department of Microbiology and Immunology, Weill Cornell Medicine, New York City, NY, USA. [10]Department of Medicine, Division of Infectious Diseases, Icahn School of Medicine at Mount Sinai, New York City, NY, USA. [11]Department of Pathology, Molecular and Cell-Based Medicine, Icahn School of Medicine at Mount Sinai New York, New York City, NY, USA. [12]The Tisch Cancer Institute, Icahn School of Medicine at Mount Sinai, New York City, NY, USA. [13]Department of Population Health Sciences, Weill Cornell Medicine, New York City, NY, USA. ✉e-mail: iliev@med.cornell.edu

Methods

Human participants

Cohort 1. Blood from 121 patients diagnosed with SARS-CoV-2 infection at Weill Cornell Medicine (NewYork Presbyterian and Lower Manhattan Hospital) was collected under the institutional review board (IRB) 20-03021645 and IRB 20-03021671 between March 2020 and June 2020. Participants were recruited from the inpatient division of NewYork Presbyterian Hospital and the Weill Cornell Medicine pulmonary and post-ICU clinics. For 91 patients (25 mild/moderate and 66 severe), only blood samples were collected, allowing for measurement of fungal antibodies and calprotectin (Extended Data Table 1, Figs. 1 and 3a and Extended Data Fig. 1). For the rest of the patients with COVID-19 of this cohort (30 patients divided into 17 mild/moderate and 13 severe), PBMCs were used for multidimensional flow cytometry as described previously[29] and measurement of fungal antibodies (Extended Data Table 1, Fig. 3b,c and Extended Data Fig. 3). All patients were classified as mild/moderate (mCOVID-19) and severe (sCOVID-19) disease according with oxygen requirements with mild/moderate disease defined as SARS-CoV-2 infection and <6 l noninvasive supplemental oxygen to maintain SpO_2 > 92%, and severe disease defined as SARS-CoV-2 infection requiring hospitalization and received >6 l supplemental oxygen or mechanical ventilation[29]. Blood samples from 36 SARS-CoV-2-negative individuals defined as the absence of clinical symptoms and negative for SARS-COV-2 spike receptor binding domain (RBD) IgG were used as 'define control' (HD; Extended Data Table 1, Figs. 1 and 3a and Extended Data Fig. 1). Serum from 39 patients with CD collected at Weill Cornell Medicine was used as CD ASCA positive controls. Antifungal antibodies were measured in plasma from all individuals. Throughout the study, mild and moderate cases (mCOVID-19) were grouped together for analysis against severe cases (sCOVID-19) or uninfected participants (HD) except in Fig. 1a, where all patients with COVID-19 were pulled together for comparison against patients with CD and uninfected controls. Sample size was not statistically predetermined.

Clinical severity at the time of sample collection was assessed using the World Health Organization (WHO) eight-category ordinal scale, which is as follows: (1) not hospitalized and no limitations of activities; (2) not hospitalized, with limitation of activities, home oxygen requirement, or both; (3) hospitalized, not requiring supplemental oxygen and no longer requiring ongoing medical care (used if hospitalization was extended for infection-control or other nonmedical reasons); (4) hospitalized, not requiring supplemental oxygen but requiring ongoing medical care (related to COVID-19 or to other medical conditions); (5) hospitalized, requiring any supplemental oxygen; (6) hospitalized, requiring noninvasive ventilation or use of high-flow oxygen devices; (7) hospitalized, receiving invasive mechanical ventilation or extracorporeal membrane oxygenation and (8) death[51].

Cohort 2. Blood from patients diagnosed with SARS-CoV-2 infection at Weill Cornell Medicine (NewYork Presbyterian and Lower Manhattan Hospital) was collected under IRB 20-03021645 and IRB 20-03021671 between March 2020 and March 2021. Participants were recruited from the inpatient division of NewYork Presbyterian Hospital and the Weill Cornell Medicine pulmonary and post-ICU clinics as described in ref. 34. Samples from a total of 39 participants including healthy individuals (HD, defined as absence of clinical symptoms and negative for SARS-COV-2 spike RBD IgG), recovered patients with sCOVID-19 (WHO score 6–7, sCOVID-19), and recovered non-COVID-19 critically ill patients (non-COVID-19) were used for plasma and $CD34^+$ cell isolation (Extended Data Table 2). Twenty-six of these 39 participants were followed after recovery from mild/moderate (mCOVID-19) or severe (sCOVID-19) COVID-19 and were partitioned into an early recovery group (2–4 months following admission, 'early') and a late recovery group (4–12 months following admission, 'late') as described in ref. 34.

Cohort 3. This cohort consisted of ten patients with COVID-19 treated as inpatients at Weill Cornell Medicine NewYork Presbyterian Hospital, between January and April 2021. Sample size was not statistically predetermined. Blood and fecal samples were collected under IRB 20-03021645. Ten SARS-CoV-2-negative individuals defined as by absence of clinical symptoms were used as uninfected controls (HD). Clinical severity at the time of fecal sample collection was assessed using the WHO eight-category ordinal scale as above.

Human sample processing and gut fungal strain isolation. Patient samples were handled under Biosafety Level 2^+ containment conditions following risk assessments and code of practice approved by Weill Cornell Medicine. Blood samples in serum separator tubes were centrifuged at 1,500*g* for 10 min, and serum was aliquoted and stored at −80 °C. Aliquots of blood from heparin tubes were stained for whole-blood flow cytometry panels (Flow cytometry) or centrifuged at 2,000*g* for 10 min and plasma was stored at −80 °C. Fresh human fecal samples collected from patients with COVID-19 were diluted in sterile PBS and plated onto Sabouraud dextrose agar (SDA), supplemented with penicillin–streptomycin (Sigma). SDA plates were incubated at 37 °C for 48 h. Fungal colonies were picked up from both cultures (37 °C, overnight). Isolated fungal colonies from each individual participant were identified by matrix-assisted laser desorption/ionization-time of flight mass spectrometer. *C. albicans* COVCa1, *C. albicans* COVCa2, *C. albicans* COVCa5 and *C. glabrata* COVCg3 were used in this study.

Fungal lysates preparation. *C. albicans* SC5314 (MYA76), *S. cerevisiae* (MYA-796), *C. parapsilosis* (22019), *A. fumigatus Fresenius* (46645) and *Malassezia restricta* (MYA-4611) were obtained from the American Type Culture Collection (ATCC). *C. albicans, C. parapsilosis* and *S. cerevisiae* were first grown on SDA plates, and then cultivated in Sabouraud Dextrose Broth (EMD Chemicals) at 37 °C in aerobic conditions overnight. *A. fumigatus* was collected after 4 d of growth on SDA plates at 30 °C and germinated in liquid media until mycelia were present. *M. restricta* was cultured on modified Dixon agar plates and cultivated in modified Dixon medium for 7 d. *C. albicans*, *C. parapsilosis*, *S. cerevisiae* and *M. restricta* were collected by centrifugation for 5 min at 330*g*. Mycelia of *A. fumigatus* were collected in filter paper.

For fungal lysate preparation, all fungal pellets were washed three times with PBS (Corning), fixed in 4% paraformaldehyde for 60 min at 4 °C. Fungal suspensions were washed three times by pelleting at 900*g* for 2 min, aspirating the supernatant and resuspending the pellet in molecular-grade water. They were treated with three freeze-thaw cycles of 10 min in dry ice and then 10 min in a 75 °C incubator. Finally, fungal suspensions were sonicated for eight cycles of 15 s on/30 s off for cell disruption. All extracts were centrifuged at 15,000*g* for 10 min to remove debris, and supernatants were stored at −330 °C until use for ELISA plate coating. The extract of *Alternaria alternata* was obtained from Greer Laboratories. The extract was resuspended in PBS, centrifuged at 15,000*g* for 10 min and supernatants were stored at −30 °C until use.

ELISA. Recombinant SARS-CoV-2 RBD protein and recombinant SARS-COV-2 spike RBD protein antibody were obtained from Abclonal. To measure the antibody against fungi, fungi lysates or yeast mannan (Sigma) were used as the coating antigen. The 96-well plates (Corning) were coated with 1 μg ml^{-1} of recombinant SARS-CoV-2 protein, 0.5 ng ml^{-1} of flagellin (Invivogen), 2.5 μg ml^{-1} of yeast mannan from *S. cerevisiae* (Sigma) or 1 μl of fungi lysates (10^9 fungi per ml) in carbonate coating buffer and incubated at 4 °C. Next, plates were washed three times with PBS containing 0.05% Tween-20 (wash buffer) and blocked with 1% BSA in PBS with 0.02% Tween-20 (PBS-T) for 1 h at room temperature. All samples were diluted at 50- to 2,000-fold dilutions followed by serial dilutions by 3 in 1% BSA PBS-T, incubated for 2 h at room temperature. Plates were washed three times with Wash Buffer. Thereafter

anti-human IgG-horseradish peroxidase (HRP) or anti-mouse IgG-HRP (SouthernBiotech) were diluted in 1% BSA in PBS-T at 1:4,000 and incubated for 1 h. Plates were washed five times with Wash Buffer, developed by the chromogenic substrate 3,3′,5,5′-tetramethylbenzidine solution (BD Biosciences). The reaction was quenched with 2 M sulfuric acid. Plates were read on a plate reader (SpectraMax Plus 384 Microplate Reader, Molecular Devices) at 450 nm and 570 nm, and optical density (ODs) were background subtracted. Endpoint titers were plotted for each specimen, and ODs, more than one-third of the maximum ODs, were considered a positive readout. Human and mouse calprotectin were quantified using BioLegend and R&D ELISA kits according to the manufacturer's instructions, respectively.

Mice. The 5-7-week-old wildtype C57BL/6J mice were originally obtained from the Jackson Laboratory. Mice were bred and maintained under specific pathogen-free (SPF) conditions. All animal care and experimental protocols were performed in accordance with the institutional animal care and use committee of Weill Cornell Medicine and Icahn School of Medicine at Mount Sinai. To establish *C. albicans* intestinal colonization in vivo experiments, mice were given drinking water supplemented with an antibiotic cocktail (0.4 g l^{-1} ampicillin, 0.4 g l^{-1} vancomycin (Gold Biotechnology), 0.4 g l^{-1} cefoperazone (Sigma)) 2 d before oral fungi colonization and continued throughout the entirety of the experiment. For intestinal fungi colonization, fungi were grown as described above, and then washed and resuspended at a concentration of 2.5×10^8 fungi per ml of PBS. Mice were orally gavaged with 5×10^7 CFU per mouse at the times indicated. To quantify fungi burden in the gut, feces were collected and suspended in PBS, serially diluted and plated on SDA plates. After overnight incubation at 37 °C in an anaerobic chamber, CFUs of fungi were counted and normalized to stool weight. For antifungal treatment, 0.5 g l^{-1} of fluconazole water (Sigma) was provided to mice ad libitum 2 d after colonization for the duration of the experiment. In the IL-6R blockade experiments, 200 µg of InVivoMAb anti-IL-6R (15A7, BioXCell) or InVivoMAb isotype control, antitrinitrophenol (2A3, BioXcell) was administered through intraperitoneal injection every other day for the duration of the experiment. One-year-old 129S1 mice were purchased from the Jackson Laboratory and housed under SPF conditions. Infection with SARS-CoV-2 was performed at the Icahn School of Medicine at Mount Sinai. Antibiotic-treated and COVCa-colonized or noncolonized 12-month-old female mice were infected intranasally with 1×10^4 PFU hCoV-19/USA (Beta, B.1.351) in 50 µl of PBS under mild Ketamin/Xylazin sedation. On day 4 after infection, animals were killed and tissue specimens were collected for analysis.

Isolation of cells from colonic lamina propria (cLP), lung and blood

cLP cells were isolated as described previously[26,52]. The middle and superior lobes of the right lung were collected after perfusion and minced, then placed for 45 min at 37 °C in 5 ml RPMI medium containing 5% FBS, liberase (100 µg ml^{-1}, Roche) and deoxyribonuclease type 1 (50 µg ml^{-1}, Sigma), 100 IU ml^{-1} penicillin and 100 µg ml^{-1} streptomycin (Thermo Fisher Scientific). The cells were recovered by disruption through a 100-µm nylon cell strainer before being centrifuged at 300*g* for 5 min. Lysis of red blood cells was performed for 2 min at room temperature before final centrifugation at 300g for 5 min and resuspension of the remaining cell pellet in 2 ml of PBS containing 1% BSA.

Blood samples were collected by cardiac puncture from a killed mouse. Cell suspensions were washed with RBC lysis buffer (BioLegend) and then centrifuged and resuspended in PBS containing 1% FBS.

Flow cytometry. High-dimensional immune cell profiling of circulating blood of patients with COVID-19 was performed as described[29]. In brief, human peripheral blood was collected in Na-heparin. Polymorphonuclear leukocytes and MO were collected by density gradient centrifugation of PBMCs, erythrocytes were lysed with BD Pharm Lyse. Peripheral blood was washed in PBS, lysed in 1× BD Pharm Lyse and washed again in PBS. PBMC cell suspensions were prepared with Ficoll-Paque following the manufacturer's protocol. Cells were stored briefly in storage media (10% FBS/1% L-glutamine/1% penicillin–streptomycin) before staining with antibody cocktails for flow cytometry. Cells were washed with PBS and then stained with dead cell dye (Fixable Viability Stain 700, BD Horizon) before washing with wash buffer (0.5% BSA/DPBS/NaN_3). Cells were then treated with 50 µl of Fc-blocking solution (2% normal rabbit serum/10% BD Fc block/PBS) before application of a 100-µl antibody cocktail diluted in wash buffer. Samples were stained within 6 h of sample collection and analyzed on a BD Biosciences FACSCanto (BD Biosciences) flow cytometer within 2 h of staining. Analysis was performed using BD FACSDiva software. Fluorophore-conjugated antibodies were used as follows: FITC-Cy7 anti-CD158e (NKB1 and DX9, BD Pharmingen), PE anti-CD158b (CH-L, BD Pharmingen), PerCP-Cy5.5 anti-CD158a (/h/g and HP-MA4, Invitrogen), PE-Vio770 anti-CD159a (NKG2A and REA110, Miltenyi Biotec), APC anti-CD158i (KIR2DS4 and JJC11.6, Miltenyi Biotec), APC-H7, PE-Cy7 and FITC anti-CD3 (SK7 (Leu-4), BD Biosciences), BV421 anti-CD56 (NCAM16.2, BD Horizon), V500C anti-CD45 (2D1, BD Biosciences), BV605 anti-CD16 (3G8, BD Horizon), PE-Cy7 anti-CD19 (J3–119; Beckman Coulter/Immunotech), PE-Cy7 anti-CD56 (N901 (NKH-1); Beckman Coulter/Immunotech), APC anti-CD11b (D12, BD Biosciences), APC-H7 anti-CD14 (MphiP9, BD Biosciences), CD124 anti-CD124 (G077F6, BioLegend), APC-H7 anti-CD8 (SK1, BD Biosciences), PE-Cy7 anti-CD4 (SK1, BD Biosciences), BV421 anti-CD19 (HIB19, BD Horizon), BV605 anti-CD5 (UCHT2, BD Horizon) and APC-H7 anti-CD20 (L27, BD Biosciences).

Fecal material was prepared by dilution and homogenization in cold sterile PBS at 25 mg ml^{-1} and strained through a 70-µm nylon mesh cell strainer. For intestinal lavage normalization, samples were centrifuged at 900*g* for 10 min, after which supernatant was transferred to a separate tube, pelleted dry weight was recorded and then resuspended at 25 mg dry weight per ml supernatant, supplementing additional volume as necessary with cold sterile PBS. In total, 50 µl of filtered fecal samples were conducted by centrifugation and resuspended in 100 µl of 4% PFA for 1 h at 4 °C. Samples were again centrifuged and aspirated, then resuspended in 100 µl of staining buffer containing both 500-fold dilution of CFW (18909-100ML-F, Sigma) and 1,000-fold dilution of SybrGreen (Sybr; S7563, Thermo Fisher Scientific) for 45 min at 4 °C. Samples were prepared for flow cytometry by resuspension in 150 µl FACS buffer (1% PFA/0.05% sodium azide) and storage at 4 °C.

Mouse flow cytometry analysis was performed as described[12,26]. Cell suspensions of mouse cells were prepared as described above, stained with different combinations of fluorochrome-conjugated antibodies in the presence of purified rat anti-mouse CD16/CD32 (BD Biosciences). Fixable Viability Dye eFluor 506 (Thermo Fisher Scientific) was used to exclude dead cells. After incubation at 4 °C for 30 min, cells were washed with FACS buffer, pelleted by centrifugation and resuspended in 200 µl of FACS buffer. Data were acquired on LSR Fortessa (BD Biosciences). Flow cytometry analysis was performed by using FlowJo (TreeStar) software using a uniform sequential gating strategy (Extended Data Fig. 2a,b). Flow cytometry data were shown as mean fluorescence intensity. Fluorophore-conjugated antibodies were used as follows: BUV395 anti-CD11b (M1/70, BD Biosciences), BV605 anti-CD4 (RM4-5, BioLegend), BV650 anti-CD45 (30-F11, BioLegend), BV711 anti-Ly-6G (1A8, BioLegend) and APC-Cy7 anti-TCRβ (H57-597, BioLegend).

Immunofluorescence staining. Tissues were processed as described previously[53,54]. Lung tissues were fixed for 48 h in 4% paraformaldehyde at 4 °C. Two days later, tissues were dehydrated in 30% sucrose overnight at 4 °C and subsequently embedded in optimal cutting temperature compound media. Frozen tissue sections were sectioned using Leica CM1850/Leica 3050S at a thickness of 20 µm. Fc receptors

were blocked with anti-CD16/32 Fc block antibody (BioLegend) diluted in PBS containing 2% serum and 2% FBS for 1 h at room temperature. Sections were stained with the antibodies; Donkey anti-goat MPO (R&D Systems), Goat anti-rabbit Histone H3 (Abcam), APC anti-Ly-6G (1A8, BioLegend) were diluted in PBS containing 2% donkey serum, 2% FBS and 0.05% Fc block for 1 h at room temperature. Sections were subsequently washed with 1× PBS and counter-stained with donkey anti-goat 488 (Invitrogen) and donkey anti-rabbit 555 (Invitrogen). Sections were coverslipped using Immun-mount mounting medium (Thermo Fisher Scientific) and cover glasses with a 0.13–0.17 mm thickness (Thermo Fisher Scientific). Fluorescence was detected with a Zeiss LSM 880 confocal microscope (Carl Zeiss) equipped with 405, 488, 514, 561, 594 and 633 nm solid-state laser lines, a 32-channel spectral detector (409–695 nm), and ×10/0.3, Plan-Apochromat ×20/0.8, ×40 and 633/1.40 objectives. Zen Black (Carl Zeiss) software suite was used for data collection. The imaging data were processed and analyzed using Imaris software version 8.3.1 (Bitplane). Image analysis was conducted on acquired images as follows: two sections per slide and two slides per animal of $n = 4–6$ animals.

Mycobiota library generation, sequencing and analysis. DNA was extracted from homogenized human fecal samples using DNA HiBind mini spin columns kit (Omega) according to the manufacturer's instructions. Fungal ITS1 sequencing and analysis have been performed as described previously[26,55].

CD34$^+$ cell isolation and single-cell RNA and ATAC sequencing. CD34$^+$ cell isolation and single-cell library preparation were performed as described previously[34]. Frozen PBMCs were thawed in a 37 °C water bath and subsequently washed with RPMI before being centrifuged. An aliquot of the PBMCs was stained with 7-AAD (BioLegend) alone for viability assessment. The remaining cells were incubated with CD34 microbeads (Miltenyi Biotec) and isolated using a magnetic column (Miltenyi Biotec) following the manufacturer's instructions. The positively selected cells were then stained with a panel of antibodies including FITC anti-CD34 (AC136, Miltenyi Biotec), Pacific Blue anti-CD49f (BioLegend, GoH3), PE anti-CD90 (5E10, BioLegend), PE/cy7 anti-CD38 (HIT2, BioLegend), APC/cy7 anti-CD45RA (HI100, BioLegend) and lineage markers (Biotin anti-CD20 (2H7), Biotin anti-CD3 (SK7), Biotin anti-CD16 (3G8), Biotin anti-CD56 (5.1H11) and Biotin anti-CD14 (M5E2), (all from BioLegend)). After incubating in the dark for 30 min, the cells were washed with PBS and subsequently incubated with Streptavidin-BV605 (BD Horizon) for another 30 min. CD34$^+$ cells were then sorted from the positive fraction, and viable PBMCs were sorted from the PBMC aliquot using a BD FACSAria cell sorter at ratios of 1:5–1:20. Nuclei were isolated from a mix of CD34$^+$ cells and PBMC according to 'Low Cell Input Nuclei Isolation' protocol (CG000365-Rev B, 10x Genomics) and were processed using Chromium Controller and Next GEM Accessory Kit (1000202, 10x Genomics) and Chromium Next GEM Single-Cell Multiome ATAC + Gene Expression Reagent Bundle (1000285, 10x Genomics) following the manufacturer's User Guide (CG000338-Rev D, 10x Genomics). Targeted nuclei recovery ranged from 5,000 to 10,000. The single-cell RNA and ATAC sequencing libraries were prepared using Dual Index Kit TT Set A (1000215, 10x Genomics) and Single Index Kit N Set A (1000212, 10x Genomics), respectively, and sequenced on Illumina NovaSeq6000 or NextSeq platform. The data analysis was performed as described in ref. 34. The data are available on the Gene Expression Omnibus (GEO) database under accession number GSE196990.

Quantification and statistical analysis. Statistics were computed using GraphPad Prism version 8.4.3 (GraphPad Software). In general, the nonparametric Mann–Whitney Wilcoxon test (which does not assume normal distribution) was used for two groups, and one-way analysis of variance with Tukey's or Kruskal–Wallis and Dunn's for multiple comparisons was used for three or more groups. For all figures statistical details specific to experiments are reported in the figure legends. Graphs display mean values with error bars that correspond to the s.e. of the mean (mean ± s.e.m.). Statistical analysis on mycobiome-related data was performed using R version 4.0.4 (R Core Team, 2014). The P value(s) reported in all figure legends are the likelihood(s) of observing the effect size(s) if the null hypothesis of zero difference is true. They are denoted as not significant $P \geq 0.05$, $^*P < 0.05$, $^{**}P < 0.01$, $^{***}P < 0.001$, $^{****}P < 0.0001$. Correlation analysis of cell frequencies and ACAL IgG levels was performed on flow cytometry-derived cellular and ELISA data, and assessed within groups of sCOVID-19 ($n = 13$) or mCOVID-19 ($n = 17$) patients using the Spearman correlation coefficient and associated statistical test. Differing correlations between severe versus mild/moderate groups were assessed by evaluating the significance of an interaction term in the linear model cell.frequency ~ antibody.level + severity + antibody.level:severity. Statistical analysis was performed using R version 4.0.4, and associated plots were generated using ggplot2.

Reporting summary

Further information on research design is available in the Nature Portfolio Reporting Summary linked to this article.

Data availability

16S and ITS sequencing data are available in the National Center for Biotechnology Information (NCBI) Sequence Read Archive with the accession code PRJNA732432. The single-cell transcriptome and ATAC sequencing data have been deposited in NCBI GEO under the accession number GSE196990. Source data are provided with this paper.

References

51. Beigel, J. H. et al. Remdesivir for the treatment of COVID-19—final report. *N. Engl. J. Med.* **383**, 1813–1826 (2020).
52. Doron, I. et al. Mycobiota-induced IgA antibodies regulate fungal commensalism in the gut and are dysregulated in Crohn's disease. *Nat. Microbiol.* **6**, 1493–1504 (2021).
53. Yeung, S. T., Ovando, L. J., Russo, A. J., Rathinam, V. A. & Khanna, K. M. CD169$^+$ macrophage intrinsic IL-10 production regulates immune homeostasis during sepsis. *Cell Rep.* **42**, 112171 (2023).
54. Ural, B. B. et al. Identification of a nerve-associated, lung-resident interstitial macrophage subset with distinct localization and immunoregulatory properties. *Sci. Immunol.* **5**, eaax8756 (2020).
55. Tang, J., Iliev, I. D., Brown, J., Underhill, D. M. & Funari, V. A. Mycobiome: approaches to analysis of intestinal fungi. *J. Immunol. Methods* **421**, 112–121 (2015).

Acknowledgements

We thank members of the Iliev Laboratory for their critical reviews of the manuscript. We thank all contributing members of the Department of Pathology and Laboratory Medicine, of the JRI IBD Live Cell Bank Consortium and the Microbiome Core Laboratory of Weill Cornell Medicine, the NYU Langone Health Microscopy Laboratory (NCI P30CA016087), Khanna Laboratory (supported by R01AI143861 and R01AI143861-02S1) and R. Albrecht, R. Cadogan, D. Flores for support with the BSL3 facility and procedures. The authors were supported by WCM WCG COVID-19; WCGS Merit Fellowship (to W.-Y.L); Asan foundation, ROK (to J.-G.C.); K08MH130773 (to C.N.P.); R01AI148416, R01AI148416-S1, R01AI148416-S2, Burrough Welcome Trust PATH Award, and the Hirschl Weill-Caulier Award (to S.Z.J); R01AI160706 and R01DK130425 (to M. Schotsaert); CRIPT, CEIRR (contract # 75N93021C00014) U19AI135972, U19AI168631 and U19AI142733 (to A.G.-S.). Research in the Iliev Laboratory is supported by the US National Institutes of Health (R01DK113136, R01DK121977 and R01AI137157), the Leona M. and Harry B. Helmsley Charitable Trust, the Irma T. Hirschl Career Scientist Award, the Research Corporation

for Science Advancement Award, the Cancer Research Institute Lloyd J. Old STAR Award, and the Burrough Welcome Trust PATH Award. I.D.I. is a fellow of the CIFAR program Fungal Kingdom—Threats and Opportunities.

Author contributions

T.K. and I.D.I. conceived and conceptualized the study. T.K., G.S., J.C., A.R., S.T.Y. and M. Schotsaert designed experiments and analyzed data. M. Salvatore was involved in the investigation, clinical samples and clinical data acquisition. T.K., W.-Y.L., J.C., G.S., G.C, S.T.Y., C.J.G., M.M., M.B.D., I.D. and G.G.P. performed experiments and acquired and analyzed data. S.R., M.C., L.W., C.N.P., Z.Z. and G.I. provided clinical samples and participated in clinical data acquisition. S.W., L.N. contributed to experimental interpretation. I.D.I., M. Salvatore, A.G.-S. and S.Z.J. supervised the study. T.K., J.C., W.-Y.L. and I.D.I. generated figures and legends from analyzed data. I.D.I. administered the project and acquired funding. T.K. and I.D.I. wrote the manuscript.

Competing interests

The AGS Laboratory has received research support from GSK, Pfizer, Senhwa Biosciences, Kenall Manufacturing, Blade Therapeutics, Avimex, Johnson & Johnson, Dynavax, 7 Hills Pharma, Pharmamar, ImmunityBio, Accurius, Nanocomposix, Hexamer, N-fold LLC, Model Medicines, Atea Pharma, Applied Biological Laboratories and Merck, outside of the reported work. A.G.-S. has consulting agreements for the following companies involving cash and/or stock: Castlevax, Amovir, Vivaldi Biosciences, Contrafect, 7 Hills Pharma, Avimex, Pagoda, Accurius, Esperovax, Farmak, Applied Biological Laboratories, Pharmamar, CureLab Oncology, CureLab Veterinary, Synairgen, Paratus, Pfizer and Prosetta, outside of the reported work. A.G.-S. has been an invited speaker in meeting events organized by Seqirus, Janssen, Abbott and AstraZeneca; and is inventor on patents and patent applications on the use of antivirals and vaccines for the treatment and prevention of virus infections and cancer, owned by the Icahn School of Medicine at Mount Sinai, New York, outside of the reported work. M. Schotsaert has received unrelated research funding in sponsored research agreements from ArgenX BV, Moderna, 7 Hills Pharma and Phio Pharmaceuticals, which has no competing interest with this work. The other authors declare no competing interests related to this study.

Additional information

Extended data is available for this paper at https://doi.org/10.1038/s41590-023-01637-4.

Supplementary information The online version contains supplementary material available at https://doi.org/10.1038/s41590-023-01637-4.

Correspondence and requests for materials should be addressed to Iliyan D. Iliev.

Peer review information *Nature Immunology* thanks Gordon Brown and the other, anonymous, reviewer(s) for their contribution to the peer review of this work. Primary Handling Editor: Ioana Visan, in collaboration with *the Nature Immunology* team.

https://doi.org/10.1038/s41590-023-01637-4

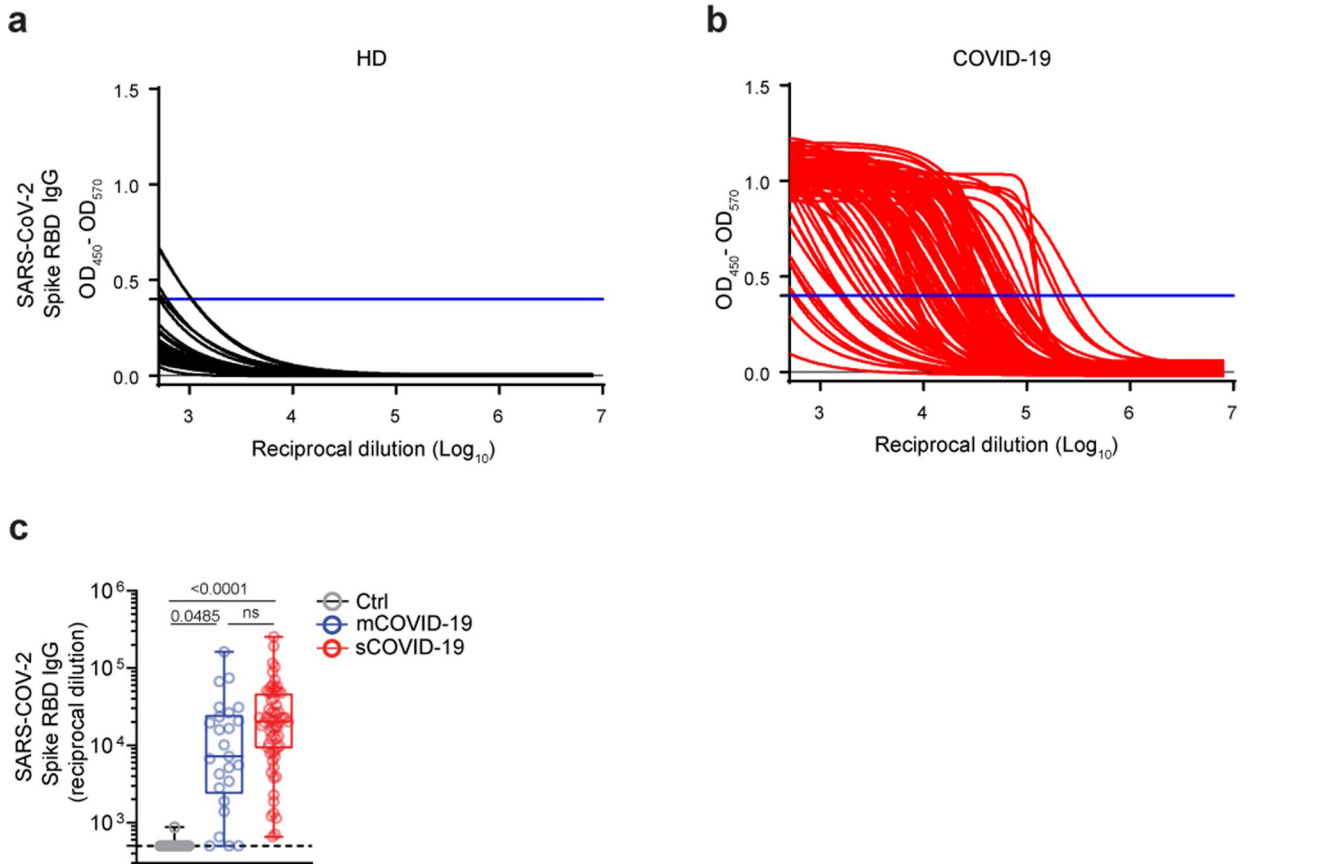

Extended Data Fig. 1 | Serological testing in Cohorts 1 and 2. a-b, SARS-CoV-2 RBD IgG titration curves in HD (n = 36, **a**) and sCOVID-19 (n = 66, **b**). c, Plasma IgG antibody titers to SARS-CoV-2 RBD in HD (n = 36), mCOVID-19 (n = 25) and sCOVID-19 (n = 66) (Extended Data Table 1). The data are shown as endpoint titers normalized to ELISA reciprocal dilution as in **a** and **b**. The dotted line indicates the limit of detection. In the boxplots, the center is drawn through the median of the measurement, and the lower and upper bounds of the box correspond to the first and third quartile. The whiskers go down to the smallest value and up to the largest. Statistical significance was determined by the one-way ANOVA followed by Tukey's multiple-comparison. Related to Fig. 1.

https://doi.org/10.1038/s41590-023-01637-4

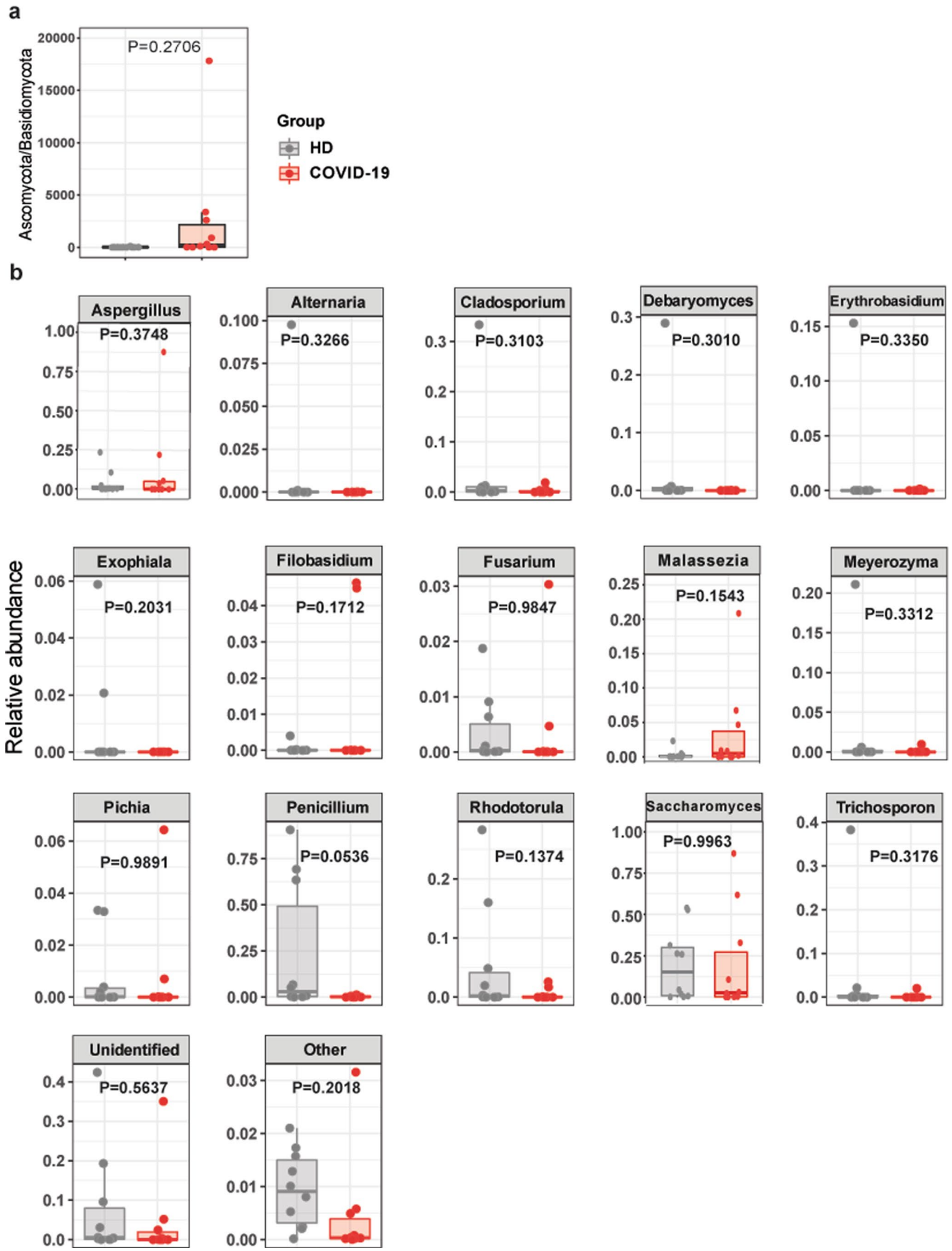

Extended Data Fig. 2 | Compositional analysis of gut mycobiota. a-b, Ratio between Ascomycota and Basidiomycota (**a**) and relative abundance of fungal species (**b**) in ITS1 sequencing of fungal rDNA from stool samples of HD (n = 10) and COVID-19 patients (n = 10). Lower and upper hinges correspond to the first and third quartile; dots represent individual patients' samples. P values were calculated using a two-tailed Mann-Whitney testing between all groups. Related to Fig. 2.

https://doi.org/10.1038/s41590-023-01637-4

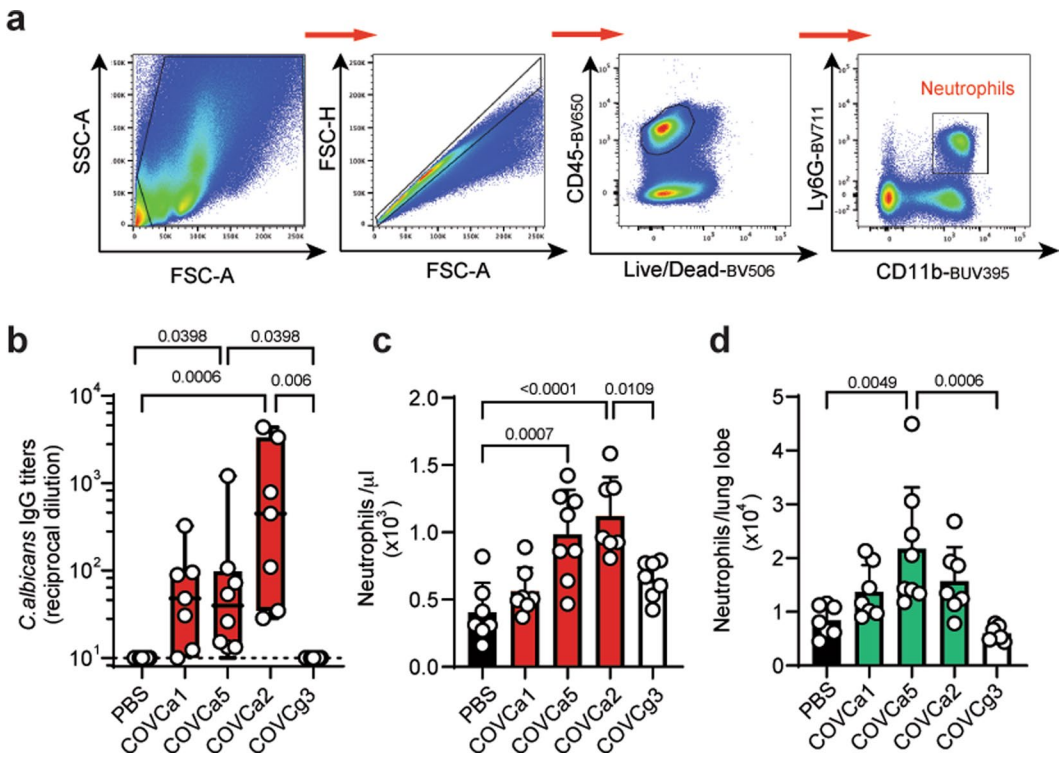

Extended Data Fig. 3 | Immune responses to C.albicans isolates from COVID-19 patients. a, Representative graphs depicting the flow cytometry gating strategy for defining murine neutrophil populations in tissues. **b-d**, Anti-C. albicans specific IgG titers (**b**), the amount of neutrophils in peripheral blood (**c**) and lung (**d**) in antibiotic-treated mice orally gavaged or not (PBS, n = 7) with either C. glabrata (CgCOV3, n = 7) or C. albicans (CaCOV1, CaCOV5, CaCOV2, n = 7) isolated from COVID-19 patient's stool. Immune responses were assessed at 2 weeks after colonization. In boxplots in **b**, the center is drawn through the median of the measurement, and the lower and upper bounds of the box correspond to the first and third quartile. The whiskers go down to the smallest value and up to the largest. The bar graphs in **c** and **d** presented as mean ± SEM. The results were pooled from two experiments. P values were calculated using the one-way ANOVA followed by Tukey's multiple comparison. ns = not significant. Related to Figs. 2 and 3.

https://doi.org/10.1038/s41590-023-01637-4

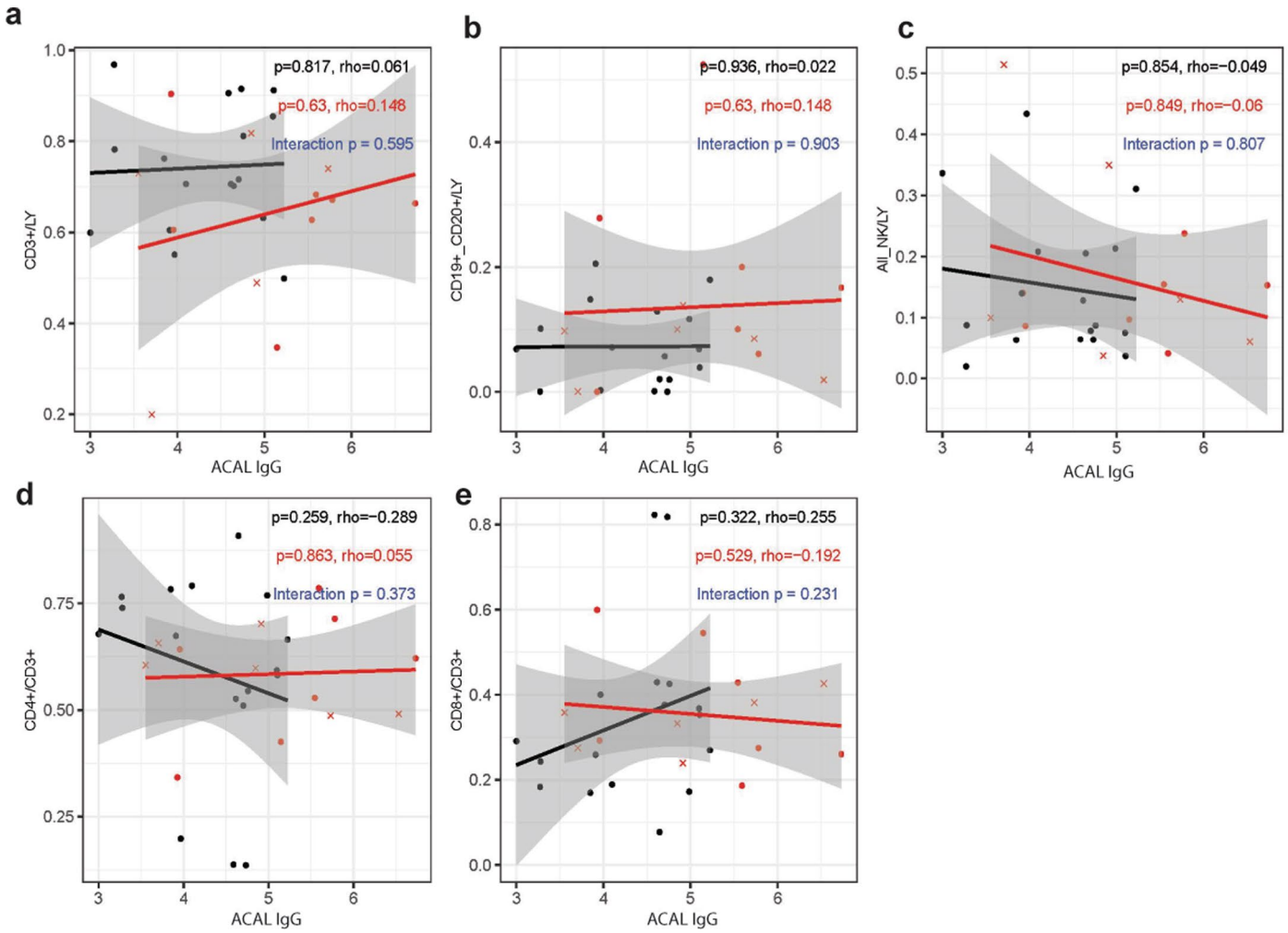

Extended Data Fig. 4 | Linear regression analysis of the Immune cell frequencies and levels of ACAL IgG in peripheral blood of mCOVID-19 and sCOVID-19. a-e, Comparison of linear regression analysis of CD3+ T cell (**a**), CD19+CD20+ B cell (**b**), NK cell (**c**), CD4+ T cell (**d**) and CD8+ T cell (**e**) frequencies and levels of ACAL IgG in peripheral blood of sCOVID-19 (n = 13) and mCOVID-19 (n = 17), see Extended Data Table 1. Crosses indicate deceased patients. Red and black lines show linear fits within severe and low to moderate groups, respectively, with 95% confidence intervals shown in gray. Spearman correlation estimates (rho) and associated p values are shown in red and black for sCOVID-19 and mCOVID19, respectively. Related to Fig. 3.

https://doi.org/10.1038/s41590-023-01637-4

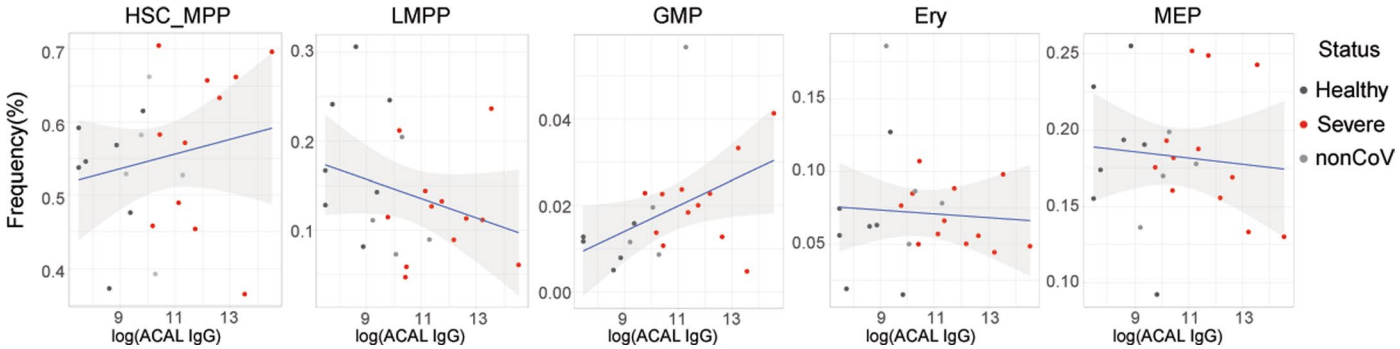

Extended Data Fig. 5 | Strong correlation between ACAL IgG and GMPs among multiple progenitor cell types. Correlation and linear regression of frequency of hematopoietic stem cells/multipotent progenitor cells (HSC/MPP), lymphoid-primed multipotent progenitor cells (LMPP), granulocyte-macrophage progenitor cells (GMP), erythroid progenitor cells (Ery), megakaryocyte-erythroid progenitor cells (MEP) with ACAL IgG (log10 titer) in enrichment of CD34+ HSPC from PBMC of HD(n = 5), sCOVID-19 (n = 12) and nonCOV-19 (n = 5), see Extended Data Table 2. Blue line indicates the regression line for all patients. The associated linear regression equation, Pearson's correlation. Coefficient and significance are shown. Related to Fig. 4.

https://doi.org/10.1038/s41590-023-01637-4

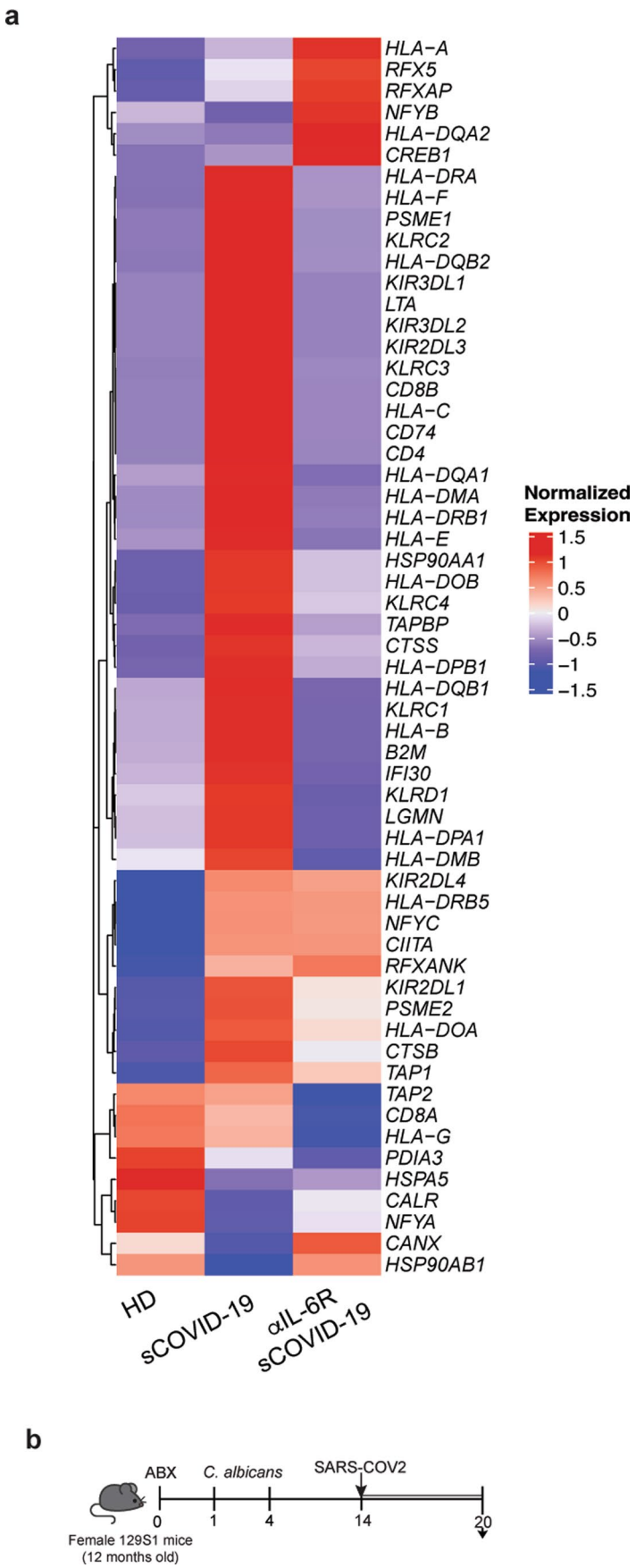

Extended Data Fig. 6 | See next page for caption.

https://doi.org/10.1038/s41590-023-01637-4

Extended Data Fig. 6 | HLA-related transcriptional signatures of GMPs form HD, sCOVID19 and sCOVID19 treated with tocilizumab. a, Heatmap showing antigen presentation marker that are differentially expressed in GMP of HD (n = 7) and sCOVID-19 who received (n = 6) or not (n = 7) IL-6R blockade treatment. Data are average of normalized expression for each gene in each group. **b**, Antibiotic treated mice were colonized with C. albicans CaCOV5 by oral gavage twice for two weeks prior to SARS-COV-2 challenge and were harvested at Day 20. Water with or without antifungal fluconazole was provided to mice two days after second oral gavage. Related to Fig. 5.

https://doi.org/10.1038/s41590-023-01637-4

Extended Data Table 1 | Clinical characteristics of cohort 1

Cohort1	HD(36)	mCOVID-19 (42)	sCOVID-19 (79)
Serological test (n)	**(36)**	**(25)**	**(66)**
Age,y, median(IQR)	54.5(51-60)	61.7(45-77)	66.6(61-74)
Sex			
Male, no.(%)	16(44.4)	10(40.0)	45(68.2)
Female, no.(%)	20(55.6)	15(60.0)	21(31.8)
Cellular analysis(n)		**(17)**	**(13)**
Age,y, median(IQR)		62.0(50-73)	63.0(49-73)
Sex			
Male, no.(%)		10(58.8)	8(61.5)
Female, no.(%)		7(41.2)	5(38.5)

https://doi.org/10.1038/s41590-023-01637-4

Extended Data Table 2 | Clinical characteristics of cohort 2

Cohort2	HD(8)	mCOVID-19 (7)	sCOVID-19 (19)	nonCOV(5)
Age,y, median(IQR)	61.3(58.75-70)	44.3(34.5-70)	57.9(60-74)	68(65-70)
Sex				
Male, no.(%)	4(50)	3(42.9)	15(78.9)	1(20.0)
Female, no.(%)	4(50)	4(57.1)	4(21.1)	4(80.0)
Clinical events				
Tocilizumab treatment	—	0/7(0%)	10/17(0%)	—
Month 2-4(n)		**(7)**	**(10)**	
Age,y, median(IQR)		44(34.5-55)	57.0(47.25-67.25)	
Sex				
Male, no.(%)		3(42.9)	9(90.0)	
Female, no.(%)		4(57.1)	1(10.0)	
Month 4-12(n)		**(5)**	**(14)**	
Age,y, median(IQR)		34.0(34.5-42)	55.0(44.5-65.25)	
Sex				
Male, no.(%)		2(40.0)	11(78.6)	
Female, no.(%)		3(60.0)	3(21.4)	

https://doi.org/10.1038/s41590-023-01637-4

Extended Data Table 3 | Clinical characteristics of cohort 3

	Healthy (10)	COVID-19 (10)
Age,y, median(IQR)	49.9(41.75-58.75)	61.5(55.5-69.5)
Sex		
Male, no.(%)	5(50.0)	9(90.0)
Female, no.(%)	5(50.0)	1(10.0)

https://doi.org/10.1038/s41590-023-01637-4

Extended Data Table 4 | Antimicrobial treatment and *Candida* spp. isolation from COVID-19 patients in cohort 3

COVID-19 Patients (Cohort1)	Stool collection days (Days from hospitalization)	Antibiotics	Antifungal	Candida species (by MALDI)
Patient A	13	Levofloxacin 1 dose x 1 day	-	*C.albicans*
Patient B	2	-	-	*C.albicans*
Patient C	3	-	-	*C.glabrata*
Patient D	2	-	-	-
Patient E	3	Ceftriaxoe, Azithromycin 1 dose x 2 days	-	*C.albicans*
Patient F	3	-	-	-
Patient G	6	-	-	*C.albicans*
Patient H	3	Ceftriaxoe, Azithromycin 1 dose x 1 day	-	-
Patient I	3	-	-	*C.albicans*
Patient J	3	-	-	*C.albicans*

nature research

Corresponding author(s): Iliyan D. Iliev

Last updated by author(s): Sep 3, 2023

Reporting Summary

Nature Research wishes to improve the reproducibility of the work that we publish. This form provides structure for consistency and transparency in reporting. For further information on Nature Research policies, see Authors & Referees and the Editorial Policy Checklist.

Statistics

For all statistical analyses, confirm that the following items are present in the figure legend, table legend, main text, or Methods section.

n/a	Confirmed
☐	☒ The exact sample size (*n*) for each experimental group/condition, given as a discrete number and unit of measurement
☐	☒ A statement on whether measurements were taken from distinct samples or whether the same sample was measured repeatedly
☐	☒ The statistical test(s) used AND whether they are one- or two-sided *Only common tests should be described solely by name; describe more complex techniques in the Methods section.*
☐	☒ A description of all covariates tested
☐	☒ A description of any assumptions or corrections, such as tests of normality and adjustment for multiple comparisons
☐	☒ A full description of the statistical parameters including central tendency (e.g. means) or other basic estimates (e.g. regression coefficient) AND variation (e.g. standard deviation) or associated estimates of uncertainty (e.g. confidence intervals)
☐	☒ For null hypothesis testing, the test statistic (e.g. *F*, *t*, *r*) with confidence intervals, effect sizes, degrees of freedom and *P* value noted *Give P values as exact values whenever suitable.*
☒	☐ For Bayesian analysis, information on the choice of priors and Markov chain Monte Carlo settings
☒	☐ For hierarchical and complex designs, identification of the appropriate level for tests and full reporting of outcomes
☒	☐ Estimates of effect sizes (e.g. Cohen's *d*, Pearson's *r*), indicating how they were calculated

Our web collection on statistics for biologists contains articles on many of the points above.

Software and code

Policy information about availability of computer code

Data collection	Fungal microbiome was analyzed using the Illumina MiSeq Next generation sequencing platform. All flow cytometry data were collected by FACS Diva Software. ELISA data were collected by softmax pro 6.4.
Data analysis	Fungal microbiome analysis performed with QIIME v1.9.1 and the R packages Phyloseq (1.26.1), and Vegan (2.5-5) in R version 3.5.2 . The dendrogram performed by SNPRelate R package and circlize R package . Flow cytometry data analyzed by FlowJo V10. Statistical analysis analyzed by R and Graphpad Prism V9.5.1 software.

For manuscripts utilizing custom algorithms or software that are central to the research but not yet described in published literature, software must be made available to editors/reviewers. We strongly encourage code deposition in a community repository (e.g. GitHub). See the Nature Research guidelines for submitting code & software for further information.

Data

Policy information about availability of data

All manuscripts must include a data availability statement. This statement should provide the following information, where applicable:

- Accession codes, unique identifiers, or web links for publicly available datasets
- A list of figures that have associated raw data
- A description of any restrictions on data availability

16S and ITS sequencing data are available in the NCBI Sequence Read Archive (SRA) with the accession code PRJNA732432. The single-cell transcriptome and ATAC sequencing data have been deposited in NCBI Gene Expression Omnibus (GEO) under the accession number GSE196990.

Field-specific reporting

Please select the one below that is the best fit for your research. If you are not sure, read the appropriate sections before making your selection.

☒ Life sciences ☐ Behavioural & social sciences ☐ Ecological, evolutionary & environmental sciences

For a reference copy of the document with all sections, see nature.com/documents/nr-reporting-summary-flat.pdf

Life sciences study design

All studies must disclose on these points even when the disclosure is negative.

Sample size	Two-hundred sixteen plasma, 65 PBMC and 20 fecal samples were obtained from collections at Weill Cornell Medicine. Sample sizes were based on previous experience (Ref 29, 34) and were optimally utilized to extract as much information as possible based on resource availability to provide enough statistic robustness, reproducibility. For mouse, five or more mice per group were used in each experiment.
Data exclusions	No mice or human subject data were excluded from the analysis.
Replication	Findings in all ELISA experiments from human and mouse samples have been replicated from two independent experiments to confirm technical reproducibility. All mouse experiments in Fig.2,3 and 5 were performed at least twice.
Randomization	Randomization was not preformed with human samples as this is not an approach taken in observational studies. Patients were stratified by disease severity using disease severity scores, mild/moderate and severe. Disease scores were according with oxygen requirements with mild/moderate disease defined as SARS-CoV-2 infection and <6 liters noninvasive supplemental oxygen to maintain SpO2 >92%, and severe disease defined as SARS-CoV-2 infection requiring hospitalization and received >6 liters supplemental oxygen or mechanical ventilation. Mouse experiments were preformed by random assignation of age- and sex-matched mice in experimental groups at the beginning of each experiment.
Blinding	The investigators were blinded during sample and data collection in human study. In general, for mouse investigators were not blinded, as the investigator who planned the experiments, also performed them. However, we performed quantitative measurements and unbiased computational analyzes.

Reporting for specific materials, systems and methods

We require information from authors about some types of materials, experimental systems and methods used in many studies. Here, indicate whether each material, system or method listed is relevant to your study. If you are not sure if a list item applies to your research, read the appropriate section before selecting a response.

Materials & experimental systems

n/a	Involved in the study
☐	☒ Antibodies
☒	☐ Eukaryotic cell lines
☒	☐ Palaeontology
☐	☒ Animals and other organisms
☐	☒ Human research participants
☒	☐ Clinical data

Methods

n/a	Involved in the study
☒	☐ ChIP-seq
☐	☒ Flow cytometry
☒	☐ MRI-based neuroimaging

Antibodies

Antibodies used

The staining antibodies for flow cytometry were purchased from Thermo Fisher Scientific, Biolegend or BD Biosciences. Dead cells were excluded with eBioscience Fixable Viability Dye eFluor 506 (Thermo Fisher Scientific, #65-0866-14, 1;1000) or Fixable Viability Stain 700 (BD Horizon, #564997,1;1000) during surface staining. Fluorophore-conjugated antibodies against human antigens: FITC-Cy7 anti-CD158e(NKB1)(DX9) (BD Pharmingen, #555966,1:80), PE anti-CD158b(CH-L) (BD Pharmingen, #559785,20), PerCP-Cy5.5 anti-CD158a (/h/g) (HP-MA4) (Invitrogen, #45-1589-42 ,80), PE-Vio770 anti- CD159a (NKG2A) (REA110) (Miltenyi Biotec, #130-113-567,80), APC anti-CD158i (KIR2DS4)(JJC11.6) (Miltenyi Biotec, #130-092-681,20), APC-H7 anti-CD3(SK7 (Leu-4)) (BD Biosciences, #641406,30), PE-Cy7 anti-CD3(SK7 (Leu-4)) (BD Biosciences, #341101,60), FITC anti-CD3(SK7 (Leu-4)) (BD Biosciences, #349201,20), BV421 anti-CD56 (NCAM16.2) (BD Horizon, #562751,400), V500C anti-CD45(2D1) (BD Biosciences, #647450,40), BV605 anti-CD16 (3G8) (BD Horizon, #563172,20), PE-Cy7 anti-CD19(J3-119) (Beckman Coulter / Immunotech, #IM3628U,40), PE-Cy7 anti-CD56(N901(NKH-1)) (Beckman Coulter / Immunotech, #A51078,100), APC anti-CD11b(D12) (BD Biosciences, #340936,40), APC-H7 anti-CD14(MphiP9) (BD Biosciences, #643077,40), CD124 anti-CD124(G077F6) (BioLegend, #355014,50), APC-H7 anti-CD8(SK1) (BD Biosciences, #64140,40), PE-Cy7 anti-CD4(SK1) (BD Biosciences, #348799,40), BV421 anti-CD19(HIB19) (BD Horizon, #562440,40), BV605 anti-CD5(UCHT2) (BD Horizon, #563945,100), APC-H7 anti-CD20(L27) (BD Biosciences, #641405,40), FITC anti-CD34 (AC136) (Miltenyi, #130-113-178,100), Pacific Blue anti-CD49f (Biolegend)(GoH3, #313620,200), PE anti-CD90 (5E10) (Biolegend, #328110,100), PE/cy7 anti-CD38 (HIT2) (Biolegend, #303516,100), APC/cy7 anti-CD45RA (HI100) (Biolegend, #304128,400) and lineage markers (

Biotin anti-CD20 (2H7) (Biolegend, #302350,1:100), Biotin anti-CD3 (SK7) (Biolegend, #344820,1:100), Biotin anti-CD16 (3G8) Biolegend, #302004, 1:100, Biotin anti-CD56 (5.1H11) Biolegend, #362536,1:100 and Biotin anti-CD14 (M5E2), Biolegend, #301826, 1:100)
Fluorophore-conjugated antibodies against mouse antigens: BUV395 anti-CD11b (M1/70) (BD Bioscience, #563553,1:400), BV605 anti-CD4 (RM4-5) (BioLegend, #100548, 1:200), BV650 anti-CD45 (30-F11) (BioLegend, #103151,1:200), BV711 anti-Ly-6G (1A8) (BioLegend, #127643
,1:200), and APC-Cy7 anti- TCRβ (H57-597) (BioLegend, #109220,1:200).The antibodies for immunofluorescence staining were used; Donkey anti-goat MPO (R&D System), Goat anti-rabbit Histone H3 (abcam), APC anti-Ly-6G (1A8) (BioLegend), donkey anti-goat 488 (Invitrogen) and donkey anti-rabbit 555 (Invitrogen).

Validation

All antibodies were well validated commercial clones and routinely QC'ed by the manufacturer. Please refer to the spec sheets on the respective vendors' website for technical information and detail by searching the catalog numbers provided above. Additionally, all antibody were titrated for optimal dilution in the assay and confirmed cell staining worked before experiments. Antibodies that were labeled/conjugated in house undergo quality control before its use for experiments.

Animals and other organisms

Policy information about studies involving animals; ARRIVE guidelines recommended for reporting animal research

Laboratory animals	5-7-week-old wild-type SPF C57BL/6 mice (JAX:000664) and 129S1/SvImJ mice (JAX:0002448) were purchased from Jackson laboratory. All mice used in these experiments were housed with a 12-hr light/dark cycle per day at a temperature of 72±2℉, and 30-70% relative humidity.
Wild animals	No wild animals used in the study.
Field-collected samples	No field-collected samples used in the study.
Ethics oversight	Blood, fecal, lung and colon samples were obtained following Institutional-Review-Board-approved protocols from Weill Cornell Medicine and Icahn School of Medicine at Mount Sinai. All animal experiments were approved and are in accordance with the Institutional Animal Care and Use Committee guidelines at Weill Cornell Medicine and Icahn School of Medicine at Mount Sinai.

Note that full information on the approval of the study protocol must also be provided in the manuscript.

Human research participants

Policy information about studies involving human research participants

Population characteristics	Demographic information is included in Extended Data Table 1,Table 2 and Table3.
Recruitment	Cohort1: Participants were recruited from patients hospitalized at New York Presbyterian Hospital from March to June 2020. Cohort2: Participants were recruited from the inpatient division of New York-Presbyterian Hospital and the Weill-Cornell Medicine pulmonary and post-ICU clinics between March 2020 and March 2021. Some subjects were followed after recovery from mCOVID-19 or sCOVID-19 and were partitioned into an early convalescent group (2-4 months following admission) and a late convalescent group (4-12 months following admission). Cohort3: Ten COVID-19 patients that were treated as inpatients at Weill Cornell Medicine New York Presbyterian Hospital, between January and April 2021. Sample size was not statistically predetermined. Ten SARS-CoV-2 negative individuals were used as uninfected controls. All patients were classified in mCOVID-19 and sCOVID-19 according with oxygen requirements with mCOVID-19 defined as SARS-CoV-2 infection and <6 liters noninvasive supplemental oxygen to maintain SpO2 >92%, and sCOVID-19 defined as SARS-CoV-2 infection requiring hospitalization and received >6 liters supplemental oxygen or mechanical ventilation.
Ethics oversight	This research was reviewed and approved by the Institutional Review Board of Weill-Cornell Medicine (New York Presbyterian and Lower Manhattan hospitals) (#IRB 20-03021645 and #IRB 20-03021671). Informed consents were obtained from all enrolled patients and healthcare workers by trained staff and records maintained in our research database for the duration of our study.

Note that full information on the approval of the study protocol must also be provided in the manuscript.

Flow Cytometry

Plots

Confirm that:

☒ The axis labels state the marker and fluorochrome used (e.g. CD4-FITC).

☒ The axis scales are clearly visible. Include numbers along axes only for bottom left plot of group (a 'group' is an analysis of identical markers).

☒ All plots are contour plots with outliers or pseudocolor plots.

☒ A numerical value for number of cells or percentage (with statistics) is provided.

Methodology

Sample preparation	For human study, human peripheral blood was collected in Na-heparin. Polymorphonuclear leukocytes and monocytes were collected by density gradient centrifugation of PBMCs, erythrocytes were lysed with BD Pharm Lyse. Peripheral blood was washed in PBS, lysed in 1× BD Pharm Lyse, and washed again in PBS. PBMC cell suspensions were prepared with Ficoll-Paque following the manufacturer's protocol. Cells were stored briefly in storage media (10% heat-inactivated fetal bovine serum/1% L-glutamine/1% pen-strep) before staining with antibody cocktails for flow cytometry. For single-cell library preparation, frozen peripheral blood mononuclear cells (PBMCs) were thawed in a 37°C water bath and subsequently washed with RPMI before being centrifuged. An aliquot of the PBMCs was stained with 7-AAD (Biolegend) and CD34 microbeads (Miltenyi) and isolated using a magnetic column (Miltenyi) following the manufacturer's instructions. The positively-selected cells were then stained with a panel of antibodies, see method, and CD34+ cells were then sorted from the positive fraction, and viable PBMCs were sorted from the PBMC aliquot using a BD FACSAria cell sorter at ratios of 1:5-1:20. For mouse study, (1) Colons were isolated, opened longitudinally, washed and removed fecal contents and fat, and then cut into pieces. Such obtained tissues were rinsed thoroughly in Hank's Balanced Salt Solution (HBSS; Thermo Fisher Scientific) medium supplemented with 2 mM EDTA,15mM HEPES and 1mM DTT and gently shaken for 10 min at 37°C, followed washing, mincing and incubating in a RPMI medium containing 5% FBS, 0.5 mg/ml collagenase type VIII (Sigma), 5 U/ml DNase (Roche), 100 IU/ml penicillin and 100 µg/ml streptomycin (Thermo Fisher Scientific) for 60 min and filtered through a 70µm-nylon mesh cell strainer. After tissue dissociation the samples were re-suspended in a 40% Percoll solution (GE Healthcare), centrifuged at 950g for 20 min. Isolated cells at the bottom of the tube were resuspended in PBS containing 1% fetal bovine serum and used for flow cytometry analysis. (2) The middle and superior lobes of the right lung were harvested after perfusion and minced, then placed for 45 min at 37°C in 5 ml a RPMI medium containing 5% FBS, liberase (100 µg/ml; Roche) and deoxyribonuclease type 1 (DNase I) (50 µg/ml; Sigma), 100 IU/ml penicillin and 100 µg/ml streptomycin (Thermo Fisher Scientific). The cells were recovered by disruption through a 100-µm nylon cell strainer before being centrifuged at 300g for 5 min. Lysis of red blood cells was performed for 2 min at room temperature before a final centrifugation at 300 g for 5 min and resuspension of the remaining cell pellet in 2 ml of PBS containing 1% fetal bovine serum. (3)Blood samples were harvested by cardiac puncture from a euthanised mouse. Cell suspensions were washed with RBC lysis (BioLegend), followed centrifuging and resuspending in PBS containing 1% fetal bovine serum.
Instrument	Human and mouse samples were acquired on BD FACSCanto and LSRFortessa (BD Biosciences), respectively. CD34+ cells were then sorted from the positive fraction, and viable PBMCs were sorted from the PBMC aliquot using a BD FACSAria cell sorter.
Software	Flow cytometry data were collected by BD Diva and further analyzed by FlowJo V10 (TreeStar)
Cell population abundance	CD34+ cells were sorted from the positive fraction, and viable PBMCs were sorted from the PBMC aliquot at ratios of 1:5-1:20.
Gating strategy	All gating were determined after FSC/SSC gating on lymphocytes population. FSC-A vs FSC-H and SSC-A vs SSC-W gates were used to gate singlets. Only CD45 positive viable cells were included for further analysis. Additional gates to identify myeloid cell subsets are available in Extended Figure 1a,b and the previous paper (Rendeiro, A.F. et al.,Life Sci Alliance. 2020).

☒ Tick this box to confirm that a figure exemplifying the gating strategy is provided in the Supplementary Information.